A Hybrid High-Order method for the incompressible Navier-Stokes problem robust for large irrotational body forces

Daniel Castanon Quiroz*[1] and Daniele A. Di Pietro†[1]

[1]IMAG, Univ Montpellier, CNRS, Montpellier, France

December 7, 2019

Abstract

We develop a novel Hybrid High-Order method for the incompressible Navier–Stokes problem robust for large irrotational body forces. The key ingredients of the method are discrete versions of the body force and convective contributions in the momentum equation formulated in terms of a globally divergence-free velocity reconstruction. Two key properties are mimicked at the discrete level, namely the invariance of the velocity with respect to irrotational body forces and the non-dissipativity of the convective term. A full convergence analysis is carried out, showing optimal orders of convergence under a smallness condition involving only the solenoidal part of the body force. The performance of the method is illustrated by a complete panel of numerical tests, including comparisons that highlight the benefits with respect to more standard formulations.

Key words: Hybrid High-Order methods, incompressible Navier–Stokes equations, robust a priori error estimates

MSC 2010: 65N08, 65N30, 65N12, 35Q30, 76D05

1 Introduction

Let $\Omega \subset \mathbb{R}^3$ denote an open, bounded, simply connected polyhedral domain with Lipschitz boundary $\partial\Omega$. Let $\nu > 0$ be a real number representing the kinematic viscosity of the fluid, and let $\boldsymbol{f} \in L^2(\Omega)^3$ be a given vector field representing a body force. Setting $\boldsymbol{U} \coloneqq H^1_0(\Omega)^3$ and $P \coloneqq \left\{q \in L^2(\Omega) : \int_\Omega q = 0\right\}$, we consider the steady incompressible Navier–Stokes problem: Find $(\boldsymbol{u}, p) \in \boldsymbol{U} \times P$ such that

$$\nu a(\boldsymbol{u}, \boldsymbol{v}) + t(\boldsymbol{u}, \boldsymbol{u}, \boldsymbol{v}) + b(\boldsymbol{v}, p) = \ell(\boldsymbol{f}, \boldsymbol{v}) \quad \forall \boldsymbol{v} \in \boldsymbol{U}, \tag{1a}$$

$$-b(\boldsymbol{u}, q) = 0 \quad \forall q \in L^2(\Omega), \tag{1b}$$

with bilinear forms $a : \boldsymbol{U} \times \boldsymbol{U} \to \mathbb{R}$, $b : \boldsymbol{U} \times L^2(\Omega) \to \mathbb{R}$, and $\ell : L^2(\Omega)^3 \times \boldsymbol{U} \to \mathbb{R}$ defined by

$$a(\boldsymbol{w}, \boldsymbol{v}) \coloneqq \int_\Omega \nabla\boldsymbol{w} : \nabla\boldsymbol{v}, \quad b(\boldsymbol{v}, q) \coloneqq -\int_\Omega (\nabla \cdot \boldsymbol{v})q, \quad \ell(\boldsymbol{f}, \boldsymbol{v}) \coloneqq \int_\Omega \boldsymbol{f} \cdot \boldsymbol{v}, \tag{2}$$

*danielcq.mathematics@gmail.com
†daniele.di-pietro@umontpellier.fr

and trilinear form $t : \boldsymbol{U} \times \boldsymbol{U} \times \boldsymbol{U} \to \mathbb{R}$ such that

$$t(\boldsymbol{w}, \boldsymbol{v}, \boldsymbol{z}) \coloneqq \int_\Omega ((\nabla\times\boldsymbol{w}) \times \boldsymbol{v}) \cdot \boldsymbol{z}. \tag{3}$$

Above, $\nabla\cdot$ and $\nabla\times$ denote, respectively, the divergence and curl operators, while $\times$ is the cross product of two vectors. The convective term in (3) is expressed in rotational form, so p is here the so-called Bernoulli pressure, which is related to the kinematic pressure p_{kin} by the equation $p = p_{\mathrm{kin}} + \frac{1}{2}|\boldsymbol{u}|^2$.

The domain Ω being simply connected, its first Betti number is zero, and we have the following (Helmholtz–)Hodge decomposition of the body force (see, e.g., [2, Section 4.3]):

$$\boldsymbol{f} = \boldsymbol{g} + \lambda\nabla\psi, \tag{4}$$

where $\boldsymbol{g}$ is the curl of a function in $\boldsymbol{H}(\mathrm{curl};\Omega)$ whose tangent trace vanishes on $\partial\Omega$, $\psi \in H^1(\Omega)$ is such that $\|\nabla\psi\|_{L^2(\Omega)^3} = 1$, and $\lambda \in \mathbb{R}^+$. The goal of this paper is to design an optimally convergent Hybrid High-Order (HHO) discretization method for problem (1) robust with respect to large irrotational body forces, that is, for which velocity error estimates uniform in λ and independent of the pressure can be established. The robustness property should additionally be obtained *without* relying on the Hodge decomposition (4) of $\boldsymbol{f}$, which is typically not available and whose numerical approximation may be computationally expensive to obtain.

The problem considered here is related to recent works pointing out the relevance of restoring at the discrete level the L^2-orthogonality between irrotational and discretely divergence-free vector fields [36]; see also the bibliographic section therein for previous references on this subject. A lack of this orthogonality property may indeed result in poor approximations of the velocity field, whose error estimate has an adverse dependence on the pressure. In [36], the author proposes a modification of the original Crouzeix–Raviart scheme [16] where the test function in the right-hand side is replaced by an interpolate in the lowest-order Raviart–Thomas–Nédélec space [38, 41]. An extension of these ideas to arbitrary order HHO approximations of the Stokes problem is proposed in [19], where the authors derive error estimates for the velocity that are independent of the pressure and uniform in the kinematic viscosity. These ideas are further developed in [35], where the notion of discrete Helmholtz projector is introduced to achieve a similar goal in the context of classical Finite Element discretisations of the Stokes and Navier–Stokes problems; see also the recent paper [1].

The novel contribution of this work consists in extending the construction of [19] to the fully nonlinear Navier–Stokes problem, focusing on matching simplicial meshes [13]. Given an integer $k \geq 0$, the proposed method hinges on velocity unknowns that are polynomials of total degree $\leq k$ at elements and faces, and pressure unknowns that are polynomials of total degree $\leq k$ at elements. Two key ingredients ensure that the method retains the optimal convergence properties of the original HHO method while attaining robustness for large irrotational body forces, namely:

1) a reconstruction of the velocity gradient in the full space of polynomials of total degree $\leq k$ to be used, in conjunction with an HHO stabilisation, in the discretisation of the viscous term;

2) a reconstruction of the velocity in the Raviart–Thomas–Nédélec space of degree k to be used in the discretisation of the convective term and of the body force.

Both reconstructions are devised at the element level and, while the former requires the (inexpensive and embarrassingly parallel) solution of a local problem inside each element, the latter is obtained by simple prescription of the local Raviart–Thomas–Nédélec degrees of freedom. This subtle design results in error estimates for the H^1-like norm of the velocity and the L^2-norm of the pressure in h^{k+1}. These error estimates are robust with respect to large irrotational body forces in the sense made precise above, that is, they are uniform in λ and do not depend on the pressure. Notice

that a more trivial choice such as, e.g., using the Raviart–Thomas–Nédélec velocity reconstruction also for the diffusive term would result in the loss of one order of convergence. The proof of these robust estimates hinges on the discrete counterparts of two key continuous properties, namely the invariance of the velocity with respect to λ and the non-dissipativity of the convective term, and leverages an a priori bound on the velocity uniform in λ. Crucially, this bound only involves $\boldsymbol{g}$, and therefore persists in the limit $\lambda \to \infty$. Intermediate results of independent interest used in the analysis are novel Sobolev inequalities for the Raviart–Thomas–Nédélec velocity reconstruction.

The proposed ideas potentially apply to other hybrid methods for incompressible flows; see, e.g., [7, 9–11, 15, 21, 26, 33, 40, 43, 45] and references therein. In view of their tight relation with HHO methods [14], Hybridisable Discontinuous Galerkin method deserve, in particular, a more in-depth discussion, which will make the object of Remark 14 below. A point that is worth emphasising here is that even methods that produce globally divergence-free velocity approximations (as a direct output or after post-processing) *do not* automatically deliver robust error estimates. As a matter of fact, a key point consists in using globally divergence-free *test functions* for the discretisation of the body force and convective terms in the momentum balance equation, which may not be the case when the global divergence-free property for the velocity is obtained through Lagrange multipliers at faces. We also mention here virtually divergence-free numerical methods [4, 5] (see also [3, 12]). Nevertheless, they may constitute an interesting path for future research in the direction of discretisation methods robust with respect to large irrotational body forces.

The rest of the paper is organised as follows. In Section 2 we discuss three properties of the continuous problem that will play a key role at the discrete level. In Section 3 we introduce the discrete setting, including the local reconstructions at the core of the HHO method. Section 4 contains the formulation of the discrete problem and includes, in particular, the definition and properties of the novel discrete convective trilinear form. The convergence analysis is carried out in Section 5, while a complete panel of two-dimensional numerical tests is provided in Section 6, including a comparison with the standard HHO scheme of [7].

2 Three key remarks

We start by highlighting three properties of the continuous problem that will play a key role in the design and analysis of the method:

1) *velocity invariance*, which establishes that, by modifying the irrotational part of the body force in the Hodge decomposition (4), the velocity field remains unchanged;
2) *non-dissipativity of the convective term*, expressing the fact that the nonlinear term in the momentum equation does not contribute to the kinetic energy balance;
3) *uniform a priori bound on the velocity*, which establishes how the velocity solution of problem (1) is bounded only by the solenoidal component of the body force $\boldsymbol{g}$ in the decomposition (4).

2.1 Velocity invariance

Denote by $\boldsymbol{n}_\Omega$ the unit outward normal vector to $\partial\Omega$. Recalling the Hodge decomposition (4), the first property is expressed by the following relation: For all $\boldsymbol{v} \in \boldsymbol{U}$,

$$\begin{aligned} \ell(\boldsymbol{g} + \lambda\nabla\psi, \boldsymbol{v}) &= \ell(\boldsymbol{g}, \boldsymbol{v}) + \int_\Omega \lambda\nabla\psi \cdot \boldsymbol{v} \\ &= \ell(\boldsymbol{g}, \boldsymbol{v}) - \int_\Omega \lambda\psi\ (\nabla\cdot\boldsymbol{v}) + \cancel{\int_{\partial\Omega} \lambda\psi\ (\boldsymbol{v}\cdot\boldsymbol{n}_\Omega)} = \ell(\boldsymbol{g}, \boldsymbol{v}) + b(\boldsymbol{v}, \lambda\psi), \end{aligned} \tag{5}$$

where we have used the linearity of ℓ in the first equality, an integration by parts together with the strongly enforced wall boundary condition in $\boldsymbol{U}$ to cancel the boundary term in the second equality,

and we have concluded using the definition (2) of the bilinear form b. A straightforward consequence of (5) is that the velocity field is unaffected by the irrotational part of the body force, which is why we refer to this property as *velocity invariance* (with respect to λ). Mimicking (5) at the discrete level will be crucial to cancel the pressure contribution from the discretization error in Theorem 11 below; see, in particular, (76). This is, in turn, a key point to achieve robustness in λ.

2.2 Non-dissipativity of the convective term

The integration by parts formula in the following proposition generalizes [28, Lemma 6.7] to less regular functions and removes the divergence-free assumption.

Proposition 1 (Integration by parts)**.** *Let X denote a simply connected open polyhedral subset of Ω. For all $\boldsymbol{v}, \boldsymbol{w}, \boldsymbol{z} \in H^1(X)^3$, it holds*

$$\int_X ((\nabla\times\boldsymbol{w})\times\boldsymbol{v})\cdot\boldsymbol{z} = \int_X \nabla\boldsymbol{w}\boldsymbol{v}\cdot\boldsymbol{z} - \int_X \nabla\boldsymbol{w}\boldsymbol{z}\cdot\boldsymbol{v}, \tag{6}$$

where we recall that, if $\boldsymbol{y} = (y_j)_{1\le j\le 3} \in \mathbb{R}^3$, $\nabla\boldsymbol{w}\boldsymbol{y} = \sum_{j=1}^3 y_j\partial_j\boldsymbol{w}$.

Writing (6) for $X = \Omega$ and recalling the definition (3) of the trilinear form t, we obtain the second key property, namely: For any $\boldsymbol{w}, \boldsymbol{v} \in H^1(\Omega)^3$,

$$t(\boldsymbol{w},\boldsymbol{v},\boldsymbol{v}) = \int_\Omega \nabla\boldsymbol{w}\boldsymbol{v}\cdot\boldsymbol{v} - \int_\Omega \nabla\boldsymbol{w}\boldsymbol{v}\cdot\boldsymbol{v} = 0, \tag{7}$$

which expresses the fact that the convective term is *non-dissipative*, i.e., it does not contribute to the kinetic energy balance obtained taking $\boldsymbol{v} = \boldsymbol{u}$ in (1a). In Section 4.4, we will leverage (6) with X successively equal to the mesh elements to derive a reformulation of the convective term that will inspire the design of a consistent and non-dissipative discrete trilinear form. The discrete counterpart of (7), expressed by (46) below, will play a key role both in deriving an a priori bound on the discrete velocity uniform in λ (see Lemma 8) and in proving the error estimate of Theorem 11.

Proof of Proposition 1. First of all, observe that all the integrals in (6) are well-defined with the assumed regularity (use generalized Hölder inequalities with exponents $(2,4,4)$ and the embedding $H^1(X) \hookrightarrow L^4(X)$). It then suffices to prove (6) for $\boldsymbol{v}, \boldsymbol{w}, \boldsymbol{z} \in \mathcal{D}(\overline{X})^3$, the space of restrictions to X of functions that are of class C_0^∞ in an open set containing $\overline{X}$, and conclude by density.

Recalling the vector identity

$$(\nabla\times\boldsymbol{w})\times\boldsymbol{v} = \nabla\boldsymbol{w}\boldsymbol{v} - \nabla(\boldsymbol{w}\cdot\boldsymbol{v}) + (\nabla\boldsymbol{v})^\intercal\boldsymbol{w},$$

we can write

$$\int_X ((\nabla\times\boldsymbol{w})\times\boldsymbol{v})\cdot\boldsymbol{z} = \int_X \nabla\boldsymbol{w}\boldsymbol{v}\cdot\boldsymbol{z} - \int_X \nabla(\boldsymbol{w}\cdot\boldsymbol{v})\cdot\boldsymbol{z} + \int_X (\nabla\boldsymbol{v})^\intercal\boldsymbol{w}\cdot\boldsymbol{z} =: \int_X \nabla\boldsymbol{w}\boldsymbol{v}\cdot\boldsymbol{z} - \mathfrak{T}_2 + \mathfrak{T}_3. \tag{8}$$

For $\mathfrak{T}_2$, applying integration by parts we arrive at

$$\mathfrak{T}_2 = \int_{\partial X} (\boldsymbol{w}\cdot\boldsymbol{v})(\boldsymbol{z}\cdot\boldsymbol{n}) - \int_X (\boldsymbol{w}\cdot\boldsymbol{v})(\nabla\cdot\boldsymbol{z}). \tag{9}$$

For $\mathfrak{T}_3$ we can write, denoting by $\otimes$ the tensor product of vectors in $\mathbb{R}^3$,

$$\mathfrak{T}_3 = \sum_{i=1}^3\sum_{j=1}^3 \int_X \partial_i v_j w_j z_i = \int_X \nabla\boldsymbol{v} : \boldsymbol{w}\otimes\boldsymbol{z} = -\int_X \nabla\cdot(\boldsymbol{w}\otimes\boldsymbol{z})\cdot\boldsymbol{v} + \int_{\partial X} (\boldsymbol{z}\cdot\boldsymbol{n})(\boldsymbol{w}\cdot\boldsymbol{v}),$$

where the conclusion follows from an integration by parts. Using this last equation and the identity $\nabla\cdot(\boldsymbol{w}\otimes\boldsymbol{z}) = (\nabla\cdot\boldsymbol{z})\boldsymbol{w} + \nabla\boldsymbol{w}\boldsymbol{z}$, we obtain

$$\mathfrak{T}_3 = -\int_X (\nabla\cdot\boldsymbol{z})(\boldsymbol{w}\cdot\boldsymbol{v}) - \int_X \nabla\boldsymbol{w}\boldsymbol{z}\cdot\boldsymbol{v} + \int_{\partial X}(\boldsymbol{z}\cdot\boldsymbol{n})(\boldsymbol{w}\cdot\boldsymbol{v}). \tag{10}$$

Plugging (9) and (10) into (8), we finally get (6). □

2.3 Uniform a priori bound on the velocity

The third property is an a priori bound on the continuous velocity uniform in λ. Taking $\boldsymbol{v} = \boldsymbol{u}$ in (1a), $q = p - \lambda\psi$ in (1b), and summing the resulting relations, we can write

$$\nu a(\boldsymbol{u},\boldsymbol{u}) + t(\boldsymbol{u},\boldsymbol{u},\boldsymbol{u}) + b(\boldsymbol{u},p) - b(\boldsymbol{u},p-\lambda\psi) = \ell(\boldsymbol{f},\boldsymbol{u}) = \ell(\boldsymbol{g},\boldsymbol{u}) + b(\boldsymbol{u},\lambda\psi),$$

where we have used the Hodge decomposition (4) of $\boldsymbol{f}$ followed by the velocity-invariance property (5) to conclude. Simplifying the terms involving the bilinear form b in the above expression, invoking the non-dissipativity property (7) to write $t(\boldsymbol{u},\boldsymbol{u},\boldsymbol{u}) = 0$, and recalling the definition (2) of the bilinear form a, we can go on writing

$$\nu|\boldsymbol{u}|^2_{H^1(\Omega)^d} = \nu a(\boldsymbol{u},\boldsymbol{u}) = \ell(\boldsymbol{g},\boldsymbol{u}) \le \|\boldsymbol{g}\|_{L^2(\Omega)^d}\|\boldsymbol{u}\|_{L^2(\Omega)^d} \le C_{\mathrm{P}}\|\boldsymbol{g}\|_{L^2(\Omega)^d}|\boldsymbol{u}|_{H^1(\Omega)^d},$$

where C_{P} denotes a Poincaré constant in Ω. Simplifying, we arrive at

$$|\boldsymbol{u}|_{H^1(\Omega)^3} \le \nu^{-1}C_{\mathrm{P}}\|\boldsymbol{g}\|_{L^2(\Omega)^3}. \tag{11}$$

A crucial point is that, contrary to the classical estimate $|\boldsymbol{u}|_{H^1(\Omega)^3} \le \nu^{-1}C_{\mathrm{P}}\|\boldsymbol{f}\|_{L^2(\Omega)^3}$ obtained without resorting to the velocity-invariance property (5), the a priori bound (11) persists in the limit $\lambda\to\infty$. This bound, along with its discrete counterpart proved in Proposition 8, allows us to establish error estimates under the smallness assumption (68), which only concerns the solenoidal part $\boldsymbol{g}$ of the body force (see (4)).

Remark 2 (A priori bound on the pressure). It cannot be expected, in general, to have an a priori bound on the $\|p\|_{L^2(\Omega)}$ uniform in λ.

3 Discrete setting

In this section we establish the discrete setting. We start by introducing the notations for the mesh, local and broken polynomial spaces, and projectors thereon. We next define the global space of discrete velocity unknowns together with the corresponding discrete norm. Finally, discrete reconstructions of the velocity and of the gradient devised at the element level are discussed.

3.1 Mesh

We consider a refined mesh sequence $(\mathcal{T}_h)_{h>0}$ where, for a given $h>0$, $\mathcal{T}_h$ is a matching simplicial mesh characterized by the scalar $h := \max_{T\in\mathcal{T}_h} h_T$, with h_T denoting the diameter of the element $T\in\mathcal{T}_h$. The mesh sequence is assumed to be shape-regular in the usual sense; see, e.g., [13, Eq. (3.1.43)]. We denote by $\mathcal{F}_h$ the set collecting the faces of $\mathcal{T}_h$, partitioned as $\mathcal{F}_h = \mathcal{F}_h^{\mathrm{i}}\cup\mathcal{F}_h^{\mathrm{b}}$, with $\mathcal{F}_h^{\mathrm{i}}$ collecting the interfaces contained in Ω and $\mathcal{F}_h^{\mathrm{b}}$ the boundary faces contained in $\partial\Omega$. For any $T\in\mathcal{T}_h$, we denote by $\mathcal{F}_T$ the set collecting the faces of $\mathcal{F}_h$ that lie on the boundary ∂T of T and, for any $F\in\mathcal{F}_T$, we will refer with $\boldsymbol{n}_{TF}$ to the normal unit vector to F pointing outwards with respect to T.

To prevent the proliferation of generic constants we often write $a\lesssim b$ in place of $a\le Cb$ with $C>0$ independent of ν, λ, h, on the exact solution, and, for local inequalities, also on the mesh element or face. The dependencies of the hidden constant will be further specified when relevant and also in theorem statements for the sake of easy consultation.

3.2 Local and broken spaces and projectors

Let X denote a mesh element or face and, for an integer $l \geq 0$, denote by $\mathbb{P}^l(X)$ the space spanned by the restrictions to X of polynomials in the space variables of total degree $\leq l$. The L^2-orthogonal projector $\pi_X^l : L^1(X) \to \mathbb{P}^l(X)$ is such that, for all $v \in L^1(X)$,

$$\int_X (v - \pi_X^l v) w = 0 \qquad \forall w \in \mathbb{P}^l(X). \tag{12}$$

Vector and matrix versions of the L^2-orthogonal projector are obtained by applying π_X^l componentwise, and will both denoted with the bold symbol $\boldsymbol{\pi}_X^l$ in what follows. Optimal approximation properties for the L^2-orthogonal projector are proved in [20, Appendix A.2] using the classical theory of [22] (cf. also [8, Chapter 4]). Specifically, let $s \in \{0, \ldots, l+1\}$ and $r \in [1, +\infty]$. Then, it holds with hidden constant only depending on l, s, r, and the mesh regularity parameter: For all $T \in \mathcal{T}_h$, all $v \in W^{s,r}(T)$, and all $m \in \{0, \ldots, s\}$,

$$|v - \pi_T^l v|_{W^{m,r}(T)} \lesssim h_T^{s-m} |v|_{W^{s,r}(T)}, \tag{13a}$$

and, if $s \geq 1$ and $m \leq s-1$,

$$h_T^{\frac{1}{r}} |v - \pi_T^l v|_{W^{m,r}(\mathcal{F}_T)} \lesssim h_T^{s-m} |v|_{W^{s,r}(T)}, \tag{13b}$$

where $W^{m,r}(\mathcal{F}_T)$ is the space spanned by functions that are in $W^{m,r}(F)$ for all $F \in \mathcal{F}_T$, endowed with the corresponding broken norm.

At the global level, the space of broken polynomial functions on $\mathcal{T}_h$ of total degree $\leq l$ is denoted by $\mathbb{P}^l(\mathcal{T}_h)$, and π_h^l is the corresponding L^2-orthogonal projector such that, for all $v \in L^1(\Omega)$, $(\pi_h^l v)_{|T} \coloneqq \pi_T^l v_{|T}$ for all $T \in \mathcal{T}_h$. Broken polynomial spaces form subspaces of the broken Sobolev spaces

$$W^{s,r}(\mathcal{T}_h) \coloneqq \{v \in L^r(\Omega) : v_{|T} \in W^{s,r}(T) \quad \forall T \in \mathcal{T}_h\},$$

which will be used to express the regularity requirements in consistency estimates. We additionally set, as usual, $H^s(\mathcal{T}_h) \coloneqq W^{s,2}(\mathcal{T}_h)$.

3.3 Discrete spaces and norms

Let a polynomial degree $k \geq 0$ be fixed. We define the following global space of discrete velocity unknowns:

$$\underline{\boldsymbol{U}}_h^k \coloneqq \left\{ \underline{\boldsymbol{v}}_h = ((\boldsymbol{v}_T)_{T\in\mathcal{T}_h}, (\boldsymbol{v}_F)_{F\in\mathcal{F}_h}) : \boldsymbol{v}_T \in \mathbb{P}^k(T)^3 \text{ for all } T \in \mathcal{T}_h \text{ and } \boldsymbol{v}_F \in \mathbb{P}^k(F)^3 \text{ for all } F \in \mathcal{F}_h \right\}.$$

For all $\underline{\boldsymbol{v}}_h \in \underline{\boldsymbol{U}}_h^k$, we denote by $\boldsymbol{v}_h \in \mathbb{P}_h^k(\mathcal{T}_h)^3$ the vector-valued broken polynomial function obtained patching element-based unkowns, that is

$$(\boldsymbol{v}_h)_{|T} \coloneqq \boldsymbol{v}_T \quad \forall T \in \mathcal{T}_h.$$

The restrictions of $\underline{\boldsymbol{U}}_h^k$ and $\underline{\boldsymbol{v}}_h \in \underline{\boldsymbol{U}}_h^k$ to a generic mesh element $T \in \mathcal{T}_h$ are respectively denoted by $\underline{\boldsymbol{U}}_T^k$ and $\underline{\boldsymbol{v}}_T = (\boldsymbol{v}_T, (\boldsymbol{v}_F)_{F\in\mathcal{F}_T})$. The vector of discrete variables corresponding to a smooth function over Ω is obtained via the global interpolation operator $\underline{\boldsymbol{I}}_h^k : H^1(\Omega)^3 \to \underline{\boldsymbol{U}}_h^k$ such that, for all $\boldsymbol{v} \in H^1(\Omega)^3$,

$$\underline{\boldsymbol{I}}_h^k \boldsymbol{v} \coloneqq ((\boldsymbol{\pi}_T^k \boldsymbol{v}_{|T})_{T\in\mathcal{T}_h}, (\boldsymbol{\pi}_F^k \boldsymbol{v}_{|F})_{F\in\mathcal{F}_h}).$$

Its restriction to a generic mesh element $T \in \mathcal{T}_h$ is $\underline{\boldsymbol{I}}_T^k : H^1(T)^3 \to \underline{\boldsymbol{U}}_T^k$ such that, for all $\boldsymbol{v} \in H^1(T)^3$,

$$\underline{\boldsymbol{I}}_T^k \boldsymbol{v} = (\boldsymbol{\pi}_T^k \boldsymbol{v}, (\boldsymbol{\pi}_F^k \boldsymbol{v}_{|F})_{F \in \mathcal{F}_T}).$$

We furnish $\underline{\boldsymbol{U}}_h^k$ with the discrete H^1-like seminorm such that, for all $\underline{\boldsymbol{v}}_h \in \underline{\boldsymbol{U}}_h^k$,

$$\|\underline{\boldsymbol{v}}_h\|_{1,h} \coloneqq \left(\sum_{T \in \mathcal{T}_h} \|\underline{\boldsymbol{v}}_T\|_{1,T}^2 \right)^{\frac{1}{2}}, \tag{14}$$

where, for all $T \in \mathcal{T}_h$,

$$\|\underline{\boldsymbol{v}}_T\|_{1,T} \coloneqq \left(\|\nabla \boldsymbol{v}_T\|_{L^2(T)^{3\times 3}}^2 + |\underline{\boldsymbol{v}}_T|_{1,\partial T}^2 \right)^{\frac{1}{2}} \text{ with } |\underline{\boldsymbol{v}}_T|_{1,\partial T} \coloneqq \left(\sum_{F \in \mathcal{F}_T} h_F^{-1} \|\boldsymbol{v}_F - \boldsymbol{v}_T\|_{L^2(F)^3}^2 \right)^{\frac{1}{2}}. \tag{15}$$

For further use, we note the following boundedness property of the global interpolator: For all $\boldsymbol{v} \in H^1(\Omega)^3$,

$$\|\underline{\boldsymbol{I}}_h^k \boldsymbol{v}\|_{1,h} \le C_I |\boldsymbol{v}|_{H^1(\Omega)^3}, \tag{16}$$

with real number $C_I > 0$ independent of both h and $\boldsymbol{v}$. Its proof relies on the stability properties of the L^2-projectors on elements and faces proved in [20, Proposition 7.1].

The global spaces of discrete unknowns for the velocity and the pressure, respectively accounting for the wall boundary condition and the zero-average condition, are

$$\underline{\boldsymbol{U}}_{h,0}^k \coloneqq \left\{ \underline{\boldsymbol{v}}_h = ((\boldsymbol{v}_T)_{T \in \mathcal{T}_h}, (\boldsymbol{v}_F)_{F \in \mathcal{F}_h}) \in \underline{\boldsymbol{U}}_h^k : \boldsymbol{v}_F = 0 \quad \forall F \in \mathcal{F}_h^{\mathrm{b}} \right\}, \qquad P_h^k \coloneqq \mathbb{P}^k(\mathcal{T}_h) \cap P. \tag{17}$$

In the analysis, we need the following discrete Sobolev embeddings in $\underline{\boldsymbol{U}}_{h,0}^k$ (see [20, Proposition 5.4]): For all $r \in [1, 6]$ it holds, for all $\underline{\boldsymbol{v}}_h \in \underline{\boldsymbol{U}}_h^k$,

$$\|\boldsymbol{v}_h\|_{L^r(\Omega)^3} \lesssim \|\underline{\boldsymbol{v}}_h\|_{1,h}. \tag{18}$$

where the hidden constant is independent of both h and $\underline{\boldsymbol{v}}_h$, but possibly depends on Ω, k, r, and the mesh regularity parameter. It follows from (18) that the map $\|\cdot\|_{1,h}$ defines a norm on $\underline{\boldsymbol{U}}_{h,0}^k$. Classically, the corresponding dual norm of a linear form $\mathcal{L}_h : \underline{\boldsymbol{U}}_{h,0}^k \to \mathbb{R}$ is given by

$$\|\mathcal{L}_h\|_{1,h,*} \coloneqq \sup_{\underline{\boldsymbol{v}}_h \in \underline{\boldsymbol{U}}_{h,0}^k, \|\underline{\boldsymbol{v}}_h\|_{1,h}=1} \left| \mathcal{L}_h(\underline{\boldsymbol{v}}_h) \right|. \tag{19}$$

3.4 Velocity reconstruction

Robustness with respect to λ hinges on the usage of a divergence-preserving velocity reconstruction in the discretization of the body force and convective terms. Let an element $T \in \mathcal{T}_h$ be fixed, and denote by

$$\mathbb{RTN}^k(T) \coloneqq \mathbb{P}^k(T)^3 + \boldsymbol{x}\mathbb{P}^k(T)$$

the local Raviart–Thomas–Nédélec space of degree k; see [38, 41]. We define the local velocity reconstruction operator $\boldsymbol{R}_T^k : \underline{\boldsymbol{U}}_T^k \to \mathbb{RTN}^k(T)$ such that, for all $\underline{\boldsymbol{v}}_T \in \underline{\boldsymbol{U}}_T^k$,

$$\int_T \boldsymbol{R}_T^k \underline{\boldsymbol{v}}_T \cdot \boldsymbol{w} = \int_T \boldsymbol{v}_T \cdot \boldsymbol{w}, \qquad \forall \boldsymbol{w} \in \mathbb{P}^{k-1}(T)^3, \tag{20a}$$

$$\boldsymbol{R}_T^k \underline{\boldsymbol{v}}_T \cdot \boldsymbol{n}_{TF} = \boldsymbol{v}_F \cdot \boldsymbol{n}_{TF} \qquad \forall F \in \mathcal{F}_T. \tag{20b}$$

Classically, the relations (20) identify $\boldsymbol{R}_T^k$ uniquely; see, e.g., [6, Proposition 2.3.4]. Moreover, for any $\boldsymbol{v} \in H^1(T)^3$, a direct computation shows that $\boldsymbol{R}_T^k \underline{\boldsymbol{I}}_T^k \boldsymbol{v} = \boldsymbol{I}_{\mathbb{RTN},T}^k \boldsymbol{v}$, where $\boldsymbol{I}_{\mathbb{RTN},T}^k$ is the local Raviart–Thomas–Nédélec interpolator. Finally, for all $\underline{\boldsymbol{v}}_T \in \underline{\boldsymbol{U}}_T^k$, we have that

$$\begin{aligned} \|\boldsymbol{R}_T^k \underline{\boldsymbol{v}}_T - \boldsymbol{v}_T\|_{L^2(T)^3} &\lesssim \sum_{F \in \mathcal{F}_T} h_F^{\frac{1}{2}} \|(\boldsymbol{v}_F - \boldsymbol{v}_T) \cdot \boldsymbol{n}_{TF}\|_{L^2(F)} \\ &\le \sum_{F \in \mathcal{F}_T} h_F^{\frac{1}{2}} \|\boldsymbol{v}_F - \boldsymbol{v}_T\|_{L^2(F)^3} \le h_T |\underline{\boldsymbol{v}}_T|_{1,\partial T}, \end{aligned} \tag{21}$$

where the first bound follows from [19, Lemma 2], the second from a Hölder inequality along with $\|\boldsymbol{n}_{TF}\|_{L^\infty(F)^3} = 1$, and the third from the definition (15) of the $|\cdot|_{1,\partial T}$-seminorm together with $h_F \le h_T$.

Let now $\mathbb{RTN}^k(\mathcal{T}_h) \coloneqq \left\{ \boldsymbol{v} \in \boldsymbol{H}(\mathrm{div};\Omega) : \boldsymbol{v}_{|T} \in \mathbb{RTN}^k(T) \text{ for all } T \in \mathcal{T}_h \right\}$ denote the global Raviart–Thomas–Nédélec space on $\mathcal{T}_h$. A global velocity reconstruction $\boldsymbol{R}_h^k : \underline{\boldsymbol{U}}_h^k \to \mathbb{RTN}^k(\mathcal{T}_h)$ is obtained patching the local contributions: For all $\underline{\boldsymbol{v}}_h \in \underline{\boldsymbol{U}}_h^k$,

$$(\boldsymbol{R}_h^k \underline{\boldsymbol{v}}_h)_{|T} \coloneqq \boldsymbol{R}_T^k \underline{\boldsymbol{v}}_T \quad \forall T \in \mathcal{T}_h.$$

Observe that $\boldsymbol{R}_h^k \underline{\boldsymbol{v}}_h$ is well-defined, since its normal components across each mesh interface are continuous as a consequence of (20b) combined with the single-valuedness of interface unknowns, and it holds, for any $\boldsymbol{v} \in \boldsymbol{U}$, $\boldsymbol{R}_h^k \underline{\boldsymbol{I}}_h^k \boldsymbol{v} = \boldsymbol{I}_{\mathbb{RTN},h}^k \boldsymbol{v}$. Notice that the global reconstruction $\boldsymbol{R}_h^k \underline{\boldsymbol{v}}_h \in \boldsymbol{H}(\mathrm{div};\Omega)$ is merely a theoretical tool which need not be constructed in practice as, in the practical implementation, only the local reconstruction $\boldsymbol{R}_T^k \underline{\boldsymbol{v}}_T$ is needed while looping over the mesh elements.

The following proposition contains novel Sobolev inequalities for the velocity reconstruction.

Proposition 3 (Sobolev inequalities for the velocity reconstruction)**.** *It holds, for all $r \in [1,6]$ and all $\underline{\boldsymbol{v}}_h \in \underline{\boldsymbol{U}}_{h,0}^k$,*

$$\|\boldsymbol{R}_h^k \underline{\boldsymbol{v}}_h\|_{L^r(\Omega)^3} \lesssim \|\underline{\boldsymbol{v}}_h\|_{1,h}. \tag{22}$$

where the hidden constant is independent of both h and $\underline{\boldsymbol{v}}_h$, but possibly depends on Ω, k, r, and the mesh regularity parameter.

Proof. Let a mesh element $T \in \mathcal{T}_h$ be fixed. Inserting $\pm \boldsymbol{v}_T$ into the norm and using a triangle inequality, we can write

$$\|\boldsymbol{R}_T^k \underline{\boldsymbol{v}}_T\|_{L^r(T)^3} \le \|\boldsymbol{R}_T^k \underline{\boldsymbol{v}}_T - \boldsymbol{v}_T\|_{L^r(T)^3} + \|\boldsymbol{v}_T\|_{L^r(T)^3}. \tag{23}$$

Let now an integer $l \ge 0$ be fixed. From the discrete Lebesgue embeddings proved in [20, Lemma 5.1], it follows that, for all $(\alpha, \beta) \in [1, +\infty]$, all $T \in \mathcal{T}_h$, and all $v \in \mathbb{P}^l(T)$,

$$\|v\|_{L^\alpha(T)} \lesssim h_T^{\frac{3}{\alpha} - \frac{3}{\beta}} \|v\|_{L^\beta(T)}. \tag{24}$$

with hidden constant independent of h, T, and v, but possibly depending on l, α, β, and the mesh regularity parameter. Then, in the first term of (23) we get that

$$\|\boldsymbol{R}_T^k \underline{\boldsymbol{v}}_T - \boldsymbol{v}_T\|_{L^r(T)^3} \lesssim h_T^{\frac{3}{r} - \frac{3}{2}} \|\boldsymbol{R}_T^k \underline{\boldsymbol{v}}_T - \boldsymbol{v}_T\|_{L^2(T)^3} \lesssim h_T^{\frac{3}{r} - \frac{1}{2}} |\underline{\boldsymbol{v}}_T|_{1,\partial T}, \tag{25}$$

where we have used (24) with $(\alpha, \beta) = (r, 2)$ in the first inequality and the bound (21) in the second. Thus, plugging (25) into (23), raising the resulting inequality to the rth power, using the inequality $(a+b)^r \lesssim a^r + b^r$ valid for any nonnegative real numbers a and b, and summing over $T \in \mathcal{T}_h$, we get

$$\|\boldsymbol{R}_T^k \underline{\boldsymbol{v}}_T\|_{L^r(\Omega)^3}^r \lesssim \sum_{T \in \mathcal{T}_h} h_T^{\frac{6-r}{2}} |\underline{\boldsymbol{v}}_T|_{1,\partial T}^r + \|\boldsymbol{v}_h\|_{L^r(\Omega)^3}^r =: \mathfrak{T}_1 + \mathfrak{T}_2. \tag{26}$$

To estimate the first term, we distinguish two cases. If $r \in [1,2)$, denoting by h_Ω the diameter of Ω, we write

$$\begin{aligned}\mathfrak{T}_1 &= \sum_{T\in\mathcal{T}_h} h_T^r\, h_T^{\frac{3(2-r)}{2}} |\underline{\boldsymbol{v}}_T|_{1,\partial T}^r \\ &\le h_\Omega^r \sum_{T\in\mathcal{T}_h} h_T^{\frac{3(2-r)}{2}} |\underline{\boldsymbol{v}}_T|_{1,\partial T}^r \\ &\le h_\Omega^r \left(\sum_{T\in\mathcal{T}_h} h_T^3\right)^{\frac{2-r}{2}} \left(\sum_{T\in\mathcal{T}_h} |\underline{\boldsymbol{v}}_T|_{1,\partial T}^2\right)^{\frac{r}{2}} \\ &\lesssim h_\Omega^r |\Omega|^{\frac{2-r}{2}} \|\underline{\boldsymbol{v}}_T\|_{1,h}^r \lesssim \|\underline{\boldsymbol{v}}_T\|_{1,h}^r,\end{aligned} \tag{27}$$

where we have used the fact that $h_T \le h_\Omega$ to pass to the second line, a Hölder inequality with exponents $\left(\frac{2}{r}, \frac{2}{2-r}\right)$ on the sum over $T \in \mathcal{T}_h$ to pass to the third line, the mesh regularity to infer $\sum_{T\in\mathcal{T}_h} h_T^3 \lesssim \sum_{T\in\mathcal{T}_h} |T| \le |\Omega|$ along with the definitions (14) and (15) of the local and global discrete norms to pass to the fourth line, and $h_\Omega^r |\Omega|^{\frac{2-r}{2}} \lesssim 1$ to conclude. If $r \in [2,6]$, on the other hand, we write

$$\mathfrak{T}_1 = \sum_{T\in\mathcal{T}_h} h_T^{\frac{6-r}{2}} |\underline{\boldsymbol{v}}_T|_{1,\partial T}^{r-2} |\underline{\boldsymbol{v}}_T|_{1,\partial T}^2 \le h_\Omega^{\frac{6-r}{2}} \|\underline{\boldsymbol{v}}_h\|_{1,h}^{r-2} \left(\sum_{T\in\mathcal{T}_h} |\underline{\boldsymbol{v}}_T|_{1,\partial T}^2\right) \lesssim \|\underline{\boldsymbol{v}}_h\|_{1,h}^r, \tag{28}$$

where we have used $h_T \le h_\Omega$ along with $\frac{6-r}{2} \ge 0$ and $|\underline{\boldsymbol{v}}_T|_{1,\partial T} \le \|\underline{\boldsymbol{v}}_h\|_{1,h}$ along with $r-2 \ge 0$ in the first bound, and the definitions (14) and (15) of the local and global discrete norms together with $h_\Omega \lesssim 1$ to conclude.

For the second term, on the other hand, the discrete Sobolev embeddings (18) readily give

$$\mathfrak{T}_2 \lesssim \|\underline{\boldsymbol{v}}_h\|_{1,h}. \tag{29}$$

Plugging (29) and, depending on r, either (27) or (28) into (26), the conclusion follows. □

3.5 Gradient reconstruction

Let an element $T \in \mathcal{T}_h$ be fixed. For any polyomial degree $l \ge 0$, we define the local gradient reconstruction operator $\boldsymbol{G}_T^l : \underline{\boldsymbol{U}}_T^k \to \mathbb{P}^l(T)^{3\times3}$ such that, for all $\underline{\boldsymbol{v}}_T \in \underline{\boldsymbol{U}}_T^k$ and all $\boldsymbol{\tau} \in \mathbb{P}^l(T)^{3\times3}$,

$$\int_T \boldsymbol{G}_T^l \underline{\boldsymbol{v}}_T : \boldsymbol{\tau} = -\int_T \boldsymbol{v}_T \cdot (\nabla\cdot\boldsymbol{\tau}) + \sum_{F\in\mathcal{F}_T} \int_F \boldsymbol{v}_F \cdot \boldsymbol{\tau}\boldsymbol{n}_{TF}. \tag{30}$$

In (30), the right hand side is designed to resemble an integration by parts formula where the role of the function represented by $\underline{\boldsymbol{v}}_T$ is played by $\boldsymbol{v}_T$ in the volumetric term and by $\boldsymbol{v}_F$ in the boundary term. This gradient reconstruction will be used with $l = k$ in the viscous term (see Section 4.1) and with $l = 2(k+1)$ in the convective terms (see Section 4.4). The following properties hold (see [21, Proposition 1]):

(i) *Boundedness.* For all $\underline{\boldsymbol{v}}_T \in \underline{\boldsymbol{U}}_T^k$, it holds

$$\|\boldsymbol{G}_T^l \underline{\boldsymbol{v}}_T\|_{L^2(T)^{3\times3}} \lesssim \|\underline{\boldsymbol{v}}_T\|_{1,T}. \tag{31}$$

(ii) *Consistency.* For all $\boldsymbol{v} \in H^m(T)^3$ with $m = l+2$ if $l \le k$, $m = k+1$ otherwise,

$$\|\boldsymbol{G}_T^l \underline{\boldsymbol{I}}_T^k \boldsymbol{v} - \nabla\boldsymbol{v}\|_{L^2(T)^{3\times3}} + h_T^{\frac{1}{2}} \|\boldsymbol{G}_T^l \underline{\boldsymbol{I}}_T^k \underline{\boldsymbol{v}}_T - \nabla\boldsymbol{v}\|_{L^2(\partial T)^{3\times3}} \lesssim h_T^{m-1} |\boldsymbol{v}|_{H^m(T)^3}. \tag{32}$$

A global gradient reconstruction $\boldsymbol{G}_h^l : \underline{\boldsymbol{U}}_h^k \to \mathbb{P}^l(\mathcal{T}_h)^{3\times3}$ can be defined setting, for all $\underline{\boldsymbol{v}}_h \in \underline{\boldsymbol{U}}_h^k$, $(\boldsymbol{G}_h^k \underline{\boldsymbol{v}}_h)_{|T} \coloneqq \boldsymbol{G}_T^k \underline{\boldsymbol{v}}_T$ for all $T \in \mathcal{T}_h$.

4 Discrete problem

In this section, we discuss the discretization of the various term appearing in (1) along with the corresponding properties relevant for the analysis, we formulate the discrete problem, and we establish an a priori bound on the discrete velocity uniform in λ.

4.1 Viscous term

The viscous term is discretized by means of the bilinear form $a_h\colon \underline{\boldsymbol{U}}_h^k \times \underline{\boldsymbol{U}}_h^k \to \mathbb{R}$ such that, for all $\underline{\boldsymbol{w}}_h, \underline{\boldsymbol{v}}_h, \in \underline{\boldsymbol{U}}_h^k$,

$$a_h(\underline{\boldsymbol{w}}_h, \underline{\boldsymbol{v}}_h) \coloneqq \int_\Omega \boldsymbol{G}_h^k \underline{\boldsymbol{w}}_h : \boldsymbol{G}_h^k \underline{\boldsymbol{v}}_h + \sum_{T\in\mathcal{T}_h} s_T(\underline{\boldsymbol{w}}_T, \underline{\boldsymbol{v}}_T), \tag{33}$$

where, for any $T \in \mathcal{T}_h$, $s_T : \underline{\boldsymbol{U}}_T^k \times \underline{\boldsymbol{U}}_T^k \to \mathbb{R}$ denotes a local stabilization bilinear form designed according to the principles of [18, Section 4.3.1.4], so that the following properties hold:

(i) *Stability and boundedness.* There exists $C_a > 0$ independent of h (and, clearly, also of ν and λ) such that, for all $\underline{\boldsymbol{v}}_h \in \underline{\boldsymbol{U}}_h^k$,

$$C_a \|\underline{\boldsymbol{v}}_h\|_{1,h}^2 \le a_h(\underline{\boldsymbol{v}}_h, \underline{\boldsymbol{v}}_h) \le C_a^{-1} \|\underline{\boldsymbol{v}}_h\|_{1,h}^2. \tag{34}$$

(ii) *Consistency.* For all $\boldsymbol{w} \in \boldsymbol{U} \cap H^{k+2}(\mathcal{T}_h)^3$ such that $\Delta \boldsymbol{w} \in L^2(\Omega)^3$, it holds

$$\|\mathcal{E}_{a,h}(\boldsymbol{w};\cdot)\|_{1,h,*} \lesssim h^{k+1} |\boldsymbol{w}|_{H^{k+2}(\mathcal{T}_h)^3}, \tag{35}$$

where the linear form $\mathcal{E}_{a,h}(\boldsymbol{w};\cdot) : \underline{\boldsymbol{U}}_h^k \to \mathbb{R}$ representing the consistency error is such that

$$\mathcal{E}_{a,h}(\boldsymbol{w}; \underline{\boldsymbol{v}}_h) \coloneqq -\int_\Omega \Delta \boldsymbol{w} \cdot \boldsymbol{v}_h - a_h(\underline{\boldsymbol{I}}_h^k \boldsymbol{w}, \underline{\boldsymbol{v}}_h). \tag{36}$$

A classical example of stabilization bilinear form along with the proofs of properties (34) and (35) can be found in [21], to which we refer for further details.

Remark 4 (Alternative formulation). An alternative formulation with analogous properties is obtained expressing the consistent contribution in (33) in terms of a local velocity reconstruction in $\mathbb{P}^{k+1}(T)$. For further details on this choice, considered in the numerical tests of Section 6, we refer to [7].

4.2 Pressure-velocity coupling

The pressure-velocity coupling hinges on the bilinear form $b_h : \underline{\boldsymbol{U}}_h^k \times \mathbb{P}^k(\mathcal{T}_h) \to \mathbb{R}$ such that, for all $(\underline{\boldsymbol{v}}_h, q_h) \in \underline{\boldsymbol{U}}_h^k \times \mathbb{P}^k(\mathcal{T}_h)$,

$$b_h(\underline{\boldsymbol{v}}_h, q_h) \coloneqq -\int_\Omega (\nabla \cdot \boldsymbol{R}_h^k \underline{\boldsymbol{v}}_h)\, q_h. \tag{37}$$

The bilinear form b_h enjoys the following properties:

(i) *Consistency.* It holds, for all $\boldsymbol{v} \in \boldsymbol{U}$,

$$b_h(\underline{\boldsymbol{I}}_h^k \boldsymbol{v}, q_h) = b(\boldsymbol{v}, q_h) \qquad \forall q_h \in \mathbb{P}^k(\mathcal{T}_h). \tag{38}$$

(ii) *Stability.* It holds, for all $q_h \in P_h^k$, with P_h^k defined by (17),

$$\|q_h\|_{L^2(\Omega)} \lesssim \sup_{\underline{\boldsymbol{v}}_h \in \underline{\boldsymbol{U}}_{h,0}^k, \|\underline{\boldsymbol{v}}_h\|_{1,h}=1} b_h(\underline{\boldsymbol{v}}_h, q_h). \tag{39}$$

Property (38) follows observing that, by construction, $\boldsymbol{R}_h^k \underline{\boldsymbol{I}}_h^k \boldsymbol{v} = \boldsymbol{I}_{\mathbb{RTN},h}^k \boldsymbol{v}$, hence $\nabla \cdot (\boldsymbol{R}_h^k \underline{\boldsymbol{I}}_h^k \boldsymbol{v}) = \nabla \cdot (\boldsymbol{I}_{\mathbb{RTN},h}^k \boldsymbol{v}) = \pi_h^k(\nabla \cdot \boldsymbol{v})$ (see, e.g., [24, Lemma 3.7]), and the projector π_h^k can be removed since $q_h \in \mathbb{P}^k(\mathcal{T}_h)$. Property (39) classically follows from (38) using Fortin's argument (see, e.g., [24, Lemma 2.6]) after recalling the boundedness property (16) of the interpolator.

Remark 5 (Implementation). The practical implementation of the bilinear form b_h does not require the computation of the global velocity reconstruction $\boldsymbol{R}_h^k$, and relies instead on the following equivalent expression: For all $(\underline{\boldsymbol{v}}_h, q_h) \in \underline{\boldsymbol{U}}_h^k \times \mathbb{P}^k(\mathcal{T}_h)$,

$$\mathrm{b}_h(\underline{\boldsymbol{v}}_h, q_h) = \sum_{T \in \mathcal{T}_h} \left[\int_T \boldsymbol{v}_T \cdot \nabla q_T - \sum_{F \in \mathcal{F}_T} \int_F (\boldsymbol{v}_F \cdot \boldsymbol{n}_{TF}) q_T \right].$$

4.3 Body force

Denote by $\ell_h : L^2(\Omega)^3 \times \underline{\boldsymbol{U}}_h^k \to \mathbb{R}$ the bilinear form such that, for any $\boldsymbol{\phi} \in L^2(\Omega)^3$ and any $\underline{\boldsymbol{v}}_h \in \underline{\boldsymbol{U}}_h^k$,

$$\ell_h(\boldsymbol{\phi}, \underline{\boldsymbol{v}}_h) \coloneqq \int_\Omega \boldsymbol{\phi} \cdot \boldsymbol{R}_h^k \underline{\boldsymbol{v}}_h. \tag{40}$$

This bilinear form has the following properties:

(i) *Velocity invariance.* Recalling the Hodge decomposition (4) of $\boldsymbol{f}$, it holds

$$\ell_h(\boldsymbol{g} + \lambda \nabla \psi, \underline{\boldsymbol{v}}_h) = \ell_h(\boldsymbol{g}, \underline{\boldsymbol{v}}_h) + b_h(\underline{\boldsymbol{v}}_h, \lambda \pi_h^k \psi) \qquad \forall \underline{\boldsymbol{v}}_h \in \underline{\boldsymbol{U}}_{h,0}^k. \tag{41}$$

(ii) *Consistency.* For all $\boldsymbol{\phi} \in L^2(\Omega)^3 \cap H^k(\mathcal{T}_h)^3$,

$$\|\mathcal{E}_{\ell,h}(\boldsymbol{\phi}; \cdot)\|_{1,h,*} \lesssim h^{k+1} |\boldsymbol{\phi}|_{H^k(\mathcal{T}_h)^3}, \tag{42}$$

where the linear form $\mathcal{E}_{\ell,h}(\boldsymbol{\phi}; \cdot) : \underline{\boldsymbol{U}}_h^k \to \mathbb{R}$ representing the consistency error is such that

$$\mathcal{E}_{\ell,h}(\boldsymbol{\phi}; \underline{\boldsymbol{v}}_h) \coloneqq \ell_h(\boldsymbol{\phi}, \underline{\boldsymbol{v}}_h) - \int_\Omega \boldsymbol{\phi} \cdot \boldsymbol{v}_h. \tag{43}$$

The velocity invariance property (41) is the discrete counterpart of (5) and enables the cancellation of the terms involving the pressure in the expression (76) of the discretization error. It can be proved writing

$$\begin{aligned}
\ell_h(\boldsymbol{g} + \lambda \nabla \psi, \underline{\boldsymbol{v}}_h) &= \ell_h(\boldsymbol{g}, \underline{\boldsymbol{v}}_h) + \int_\Omega \lambda \nabla \psi \cdot \boldsymbol{R}_h^k \underline{\boldsymbol{v}}_h \\
&= \ell_h(\boldsymbol{g}, \underline{\boldsymbol{v}}_h) - \int_\Omega \lambda \psi \, (\nabla \cdot \boldsymbol{R}_h^k \underline{\boldsymbol{v}}_h) + \cancel{\int_{\partial\Omega} \lambda \psi \, (\boldsymbol{R}_h^k \underline{\boldsymbol{v}}_h \cdot \boldsymbol{n}_\Omega)} \\
&= \ell_h(\boldsymbol{g}, \underline{\boldsymbol{v}}_h) - \int_\Omega \lambda \pi_h^k \psi \, (\nabla \cdot \boldsymbol{R}_h^k \underline{\boldsymbol{v}}_h) \\
&= \ell_h(\boldsymbol{g}, \underline{\boldsymbol{v}}_h) + b_h(\underline{\boldsymbol{v}}_h, \lambda \pi_h^k \psi),
\end{aligned}$$

where we have used the linearity of ℓ_h along with its definition (40) in the first line, we have integrated by parts the second term and observed that the normal trace of $\boldsymbol{R}_h^k \underline{\boldsymbol{v}}_h$ vanishes on $\partial\Omega$ as a consequence of (20b) together with $\boldsymbol{v}_F = \boldsymbol{0}$ for all $F \in \mathcal{F}_h^{\mathrm{b}}$ in the second line, we have used the definition of the global L^2-orthogonal projector π_h^k after observing that $\nabla \cdot \boldsymbol{R}_h^k \underline{\boldsymbol{v}}_h \in \mathbb{P}_h^k(\mathcal{T}_h)$ in the third line, and we have recalled the definition (37) of the pressure-velocity coupling bilinear form b_h to conclude.

For the proof of the consistency property (43), we refer the reader to [17, Chapter 8].

4.4 Convective term

The discrete counterpart of the convective trilinear form t defined by (3) is designed so as to approximate, for any $\boldsymbol{w} \in \boldsymbol{U}$, the quantity

$$\ell_h((\nabla\times\boldsymbol{w})\times\boldsymbol{w},\underline{\boldsymbol{z}}_h) = \int_\Omega (\nabla\times\boldsymbol{w})\times\boldsymbol{w}\cdot\boldsymbol{R}_h^k\underline{\boldsymbol{z}}_h,$$

which naturally appears, with $\boldsymbol{w}=\boldsymbol{u}$, in the discretization error; see (76) below. Applying Proposition 1 with X successively equal to the mesh elements $T\in\mathcal{T}_h$, we can reformulate this quantity as follows:

$$\ell_h((\nabla\times\boldsymbol{w})\times\boldsymbol{w},\underline{\boldsymbol{z}}_h) = \sum_{T\in\mathcal{T}_h}\int_T (\nabla\times\boldsymbol{w})\times\boldsymbol{w}\cdot\boldsymbol{R}_T^k\underline{\boldsymbol{z}}_T = \sum_{T\in\mathcal{T}_h}\int_T \left(\nabla\boldsymbol{w}\boldsymbol{w}\cdot\boldsymbol{R}_T^k\underline{\boldsymbol{z}}_T - \nabla\boldsymbol{w}\boldsymbol{R}_T^k\underline{\boldsymbol{z}}_T\cdot\boldsymbol{w}\right). \quad (44)$$

Starting from this expression, we obtain a discrete counterpart of t by replacing inside each element the continuous velocity and gradient by the corresponding reconstructions introduced in Sections 3.4 and 3.5, respectively. Thus, we introduce the global trilinear form $t_h : \underline{\boldsymbol{U}}_h^k\times\underline{\boldsymbol{U}}_h^k\times\underline{\boldsymbol{U}}_h^k\to\mathbb{R}$ such that

$$t_h(\underline{\boldsymbol{w}}_h,\underline{\boldsymbol{v}}_h,\underline{\boldsymbol{z}}_h) \coloneqq \sum_{T\in\mathcal{T}_h} t_T(\underline{\boldsymbol{w}}_T,\underline{\boldsymbol{v}}_T,\underline{\boldsymbol{z}}_T), \quad (45a)$$

where, for any $T\in\mathcal{T}_h$, $t_T : \underline{\boldsymbol{U}}_T^k\times\underline{\boldsymbol{U}}_T^k\times\underline{\boldsymbol{U}}_T^k\to\mathbb{R}$ is defined as

$$t_T(\underline{\boldsymbol{w}}_T,\underline{\boldsymbol{v}}_T,\underline{\boldsymbol{z}}_T) \coloneqq \int_T \boldsymbol{G}_T^{2(k+1)}\underline{\boldsymbol{w}}_T\boldsymbol{R}_T^k\underline{\boldsymbol{v}}_T\cdot\boldsymbol{R}_T^k\underline{\boldsymbol{z}}_T - \int_T \boldsymbol{G}_T^{2(k+1)}\underline{\boldsymbol{w}}_T\boldsymbol{R}_T^k\underline{\boldsymbol{z}}_T\cdot\boldsymbol{R}_T^k\underline{\boldsymbol{v}}_T. \quad (45b)$$

The choice of the polynomial degree $2(k+1)$ for the gradient reconstruction is justified in the following remark.

Remark 6 (Reformulation of t_h). In the practical implementation, one does not need to compute the gradient reconstruction operators $\boldsymbol{G}_T^{2(k+1)}$ to evaluate t_h. As a matter of fact, expanding this operator in (45) according to its definition (30), we have that

$$\begin{aligned} t_h(\underline{\boldsymbol{w}}_h,\underline{\boldsymbol{v}}_h,\underline{\boldsymbol{z}}_h) = {}& \sum_{T\in\mathcal{T}_h}\left[\int_T \nabla\boldsymbol{w}_T\boldsymbol{R}_T^k\underline{\boldsymbol{v}}_T\cdot\boldsymbol{R}_T^k\underline{\boldsymbol{z}}_T - \int_T \nabla\boldsymbol{w}_T\boldsymbol{R}_T^k\underline{\boldsymbol{z}}_T\cdot\boldsymbol{R}_T^k\underline{\boldsymbol{v}}_T\right] \\ & + \sum_{T\in\mathcal{T}_h}\sum_{F\in\mathcal{F}_T}\int_F (\boldsymbol{w}_F-\boldsymbol{w}_T)\cdot\boldsymbol{R}_T^k\underline{\boldsymbol{z}}_T\left(\boldsymbol{R}_T^k\underline{\boldsymbol{v}}_T\cdot\boldsymbol{n}_{TF}\right) \\ & - \sum_{T\in\mathcal{T}_h}\sum_{F\in\mathcal{F}_T}\int_F (\boldsymbol{w}_F-\boldsymbol{w}_T)\cdot\boldsymbol{R}_T^k\underline{\boldsymbol{v}}_T\left(\boldsymbol{R}_T^k\underline{\boldsymbol{z}}_T\cdot\boldsymbol{n}_{TF}\right). \end{aligned}$$

The properties relevant for the analysis are contained in the following lemma.

Lemma 7 (Properties of t_h)**.** *The trilinear form t_h has the following properties:*

(i) Non-dissipativity. *For all $\underline{\boldsymbol{w}}_h,\underline{\boldsymbol{v}}_h\in\underline{\boldsymbol{U}}_h^k$, it holds that*

$$t_h(\underline{\boldsymbol{w}}_h,\underline{\boldsymbol{v}}_h,\underline{\boldsymbol{v}}_h) = 0. \quad (46)$$

(ii) Boundedness. *There exists a real number $C_t>0$ independent of h (and, clearly, also of ν and λ) such that, for all $\underline{\boldsymbol{w}}_h,\underline{\boldsymbol{v}}_h,\underline{\boldsymbol{z}}_h\in\underline{\boldsymbol{U}}_h^k$,*

$$|t_h(\underline{\boldsymbol{w}}_h,\underline{\boldsymbol{v}}_h,\underline{\boldsymbol{z}}_h)| \le C_t\|\underline{\boldsymbol{w}}_h\|_{1,h}\|\underline{\boldsymbol{v}}_h\|_{1,h}\|\underline{\boldsymbol{z}}_h\|_{1,h}. \quad (47)$$

(iii) Consistency. *It holds, for all* $\boldsymbol{w} \in \boldsymbol{U} \cap W^{k+1,4}(\mathcal{T}_h)^3$ *and all* $\underline{\boldsymbol{z}}_h \in \underline{\boldsymbol{U}}_h^k$,

$$\|\mathcal{E}_{t,h}(\boldsymbol{w};\cdot)\|_{1,h,*} \lesssim h^{k+1}\|\boldsymbol{w}\|_{W^{1,4}(\Omega)^3}|\boldsymbol{w}|_{W^{k+1,4}(\mathcal{T}_h)^3}, \tag{48}$$

where the linear form $\mathcal{E}_{t,h}(\boldsymbol{w};\cdot) : \underline{\boldsymbol{U}}_h^k \to \mathbb{R}$ *representing the consistency error is such that, for all* $\underline{\boldsymbol{z}}_h \in \underline{\boldsymbol{U}}_h^k$,

$$\mathcal{E}_{t,h}(\boldsymbol{w};\underline{\boldsymbol{z}}_h) \coloneqq \ell_h((\nabla\times\boldsymbol{w})\times\boldsymbol{w},\underline{\boldsymbol{z}}_h) - t_h(\underline{\boldsymbol{I}}_h^k\boldsymbol{w},\underline{\boldsymbol{I}}_h^k\boldsymbol{w},\underline{\boldsymbol{z}}_h). \tag{49}$$

Proof. (i) *Non-dissipativity.* Immediate consequence of the definition (45) of t_h.

(ii) *Boundedness.* By (45), it suffices to prove that it holds, for all $\underline{\boldsymbol{w}}_h, \underline{\boldsymbol{v}}_h, \underline{\boldsymbol{z}}_h \in \underline{\boldsymbol{U}}_h^k$,

$$\mathfrak{T} \coloneqq \left|\sum_{T\in\mathcal{T}_h}\int_T \boldsymbol{G}_T^{2(k+1)}\underline{\boldsymbol{w}}_T\boldsymbol{R}_T^k\underline{\boldsymbol{v}}_T\cdot\boldsymbol{R}_T^k\underline{\boldsymbol{z}}_T\right| \lesssim \|\underline{\boldsymbol{w}}_h\|_{1,h}\|\underline{\boldsymbol{v}}_h\|_{1,h}\|\underline{\boldsymbol{z}}_h\|_{1,h},$$

then use this bound twice with $\underline{\boldsymbol{v}}_h$ and $\underline{\boldsymbol{z}}_h$ swapped. Using Hölder inequalities with exponents $(2,4,4)$, the bound (31), and again a discrete Hölder inequality on the sum over $T \in \mathcal{T}_h$, we have that

$$\begin{aligned}
\mathfrak{T} &\lesssim \sum_{T\in\mathcal{T}_h}\|\boldsymbol{G}_T^{2(k+1)}\underline{\boldsymbol{w}}_T\|_{L^2(T)^{3\times3}}\|\boldsymbol{R}_T^k\underline{\boldsymbol{v}}_T\|_{L^4(T)^3}\|\boldsymbol{R}_T^k\underline{\boldsymbol{z}}_T\|_{L^4(T)^3}\\
&\lesssim \sum_{T\in\mathcal{T}_h}\|\underline{\boldsymbol{w}}_T\|_{1,T}\|\boldsymbol{R}_T^k\underline{\boldsymbol{v}}_T\|_{L^4(T)^3}\|\boldsymbol{R}_T^k\underline{\boldsymbol{z}}_T\|_{L^4(T)^3}\\
&\lesssim \|\underline{\boldsymbol{w}}_h\|_{1,h}\|\boldsymbol{R}_h^k\underline{\boldsymbol{v}}_h\|_{L^4(\Omega)^3}\|\boldsymbol{R}_h^k\underline{\boldsymbol{z}}_h\|_{L^4(\Omega)^3} \lesssim \|\underline{\boldsymbol{w}}_h\|_{1,h}\|\underline{\boldsymbol{v}}_h\|_{1,h}\|\underline{\boldsymbol{z}}_h\|_{1,h},
\end{aligned} \tag{50}$$

where, to bound the last two factors, we have invoked the discrete Sobolev embeddings (22) with $r = 4$.

(iii) *Consistency.* First of all, let us verify that the first term on the right hand side of (49) is well defined. By the assumed regularity, $\boldsymbol{w} \in W^{1,4}(\Omega)^3$ (combine the fact that the jumps of $\boldsymbol{w}$ vanish across interfaces since $\boldsymbol{w} \in \boldsymbol{U}$ and the regularity $\boldsymbol{w} \in W^{1,4}(\mathcal{T}_h)^3$), and we can write

$$\|(\nabla\times\boldsymbol{w})\times\boldsymbol{w}\|_{L^2(\Omega)^3} \le \|\nabla\times\boldsymbol{w}\|_{L^4(\Omega)^3}\|\boldsymbol{w}\|_{L^4(\Omega)^3} \lesssim \|\boldsymbol{w}\|_{W^{1,4}(\Omega)^3}\|\boldsymbol{w}\|_{H^1(\Omega)^3},$$

where we have concluded using the embedding $H^1(\Omega) \hookrightarrow L^4(T)$. This shows that $(\nabla\times\boldsymbol{w})\times\boldsymbol{w} \in L^2(\Omega)^3$, so this quantity legitimately appears in the first argument of ℓ_h.

Let now $\hat{\underline{\boldsymbol{w}}}_h \coloneqq \underline{\boldsymbol{I}}_h^k\boldsymbol{w}$. Using (44) and the definition (45) of t_h, we have that

$$\begin{aligned}
\mathcal{E}_{t,h}(\boldsymbol{w};\underline{\boldsymbol{v}}_h) = &\sum_{T\in\mathcal{T}_h}\int_T\left(\nabla\boldsymbol{w}\boldsymbol{w}\cdot\boldsymbol{R}_T^k\underline{\boldsymbol{z}}_T - \nabla\boldsymbol{w}\boldsymbol{R}_T^k\underline{\boldsymbol{z}}_T\cdot\boldsymbol{w}\right)\\
&+\sum_{T\in\mathcal{T}_h}\left(-\int_T\boldsymbol{G}_T^{2(k+1)}\hat{\underline{\boldsymbol{w}}}_T\boldsymbol{R}_T^k\hat{\underline{\boldsymbol{w}}}_T\cdot\boldsymbol{R}_T^k\underline{\boldsymbol{z}}_T + \int_T\boldsymbol{G}_T^{2(k+1)}\hat{\underline{\boldsymbol{w}}}_T\boldsymbol{R}_T^k\underline{\boldsymbol{z}}_T\cdot\boldsymbol{R}_T^k\hat{\underline{\boldsymbol{w}}}_T\right).
\end{aligned}$$

Inserting into the right-hand side of this last equation the quantity

$$\pm\sum_{T\in\mathcal{T}_h}\int_T\left(\boldsymbol{G}_T^{2(k+1)}\hat{\underline{\boldsymbol{w}}}_T\boldsymbol{w}\cdot\boldsymbol{R}_T^k\underline{\boldsymbol{z}}_T + \boldsymbol{G}_T^{2(k+1)}\hat{\underline{\boldsymbol{w}}}_T\boldsymbol{R}_T^k\underline{\boldsymbol{z}}_T\cdot\boldsymbol{w}\right),$$

we arrive at

$$\mathcal{E}_{t,h}(\boldsymbol{w};\underline{\boldsymbol{v}}_h) = \underbrace{\sum_{T\in\mathcal{T}_h}\int_T (\boldsymbol{G}_T^{2(k+1)}\underline{\hat{\boldsymbol{w}}}_T - \nabla\boldsymbol{w})\boldsymbol{R}_T^k\underline{\boldsymbol{z}}_T\cdot\boldsymbol{w}}_{\mathfrak{T}_1} + \underbrace{\sum_{T\in\mathcal{T}_h}\int_T (\nabla\boldsymbol{w} - \boldsymbol{G}_T^{2(k+1)}\underline{\hat{\boldsymbol{w}}}_T)\boldsymbol{w}\cdot\boldsymbol{R}_T^k\underline{\boldsymbol{z}}_T}_{\mathfrak{T}_2}$$
$$+ \underbrace{\sum_{T\in\mathcal{T}_h}\int_T \boldsymbol{G}_T^{2(k+1)}\underline{\hat{\boldsymbol{w}}}_T(\boldsymbol{w}-\boldsymbol{R}_T^k\underline{\hat{\boldsymbol{w}}}_T)\cdot\boldsymbol{R}_T^k\underline{\boldsymbol{z}}_T}_{\mathfrak{T}_3} + \underbrace{\sum_{T\in\mathcal{T}_h}\int_T \boldsymbol{G}_T^{2(k+1)}\underline{\hat{\boldsymbol{w}}}_T\boldsymbol{R}_T^k\underline{\boldsymbol{z}}_T\cdot(\boldsymbol{R}_T^k\underline{\hat{\boldsymbol{w}}}_T-\boldsymbol{w})}_{\mathfrak{T}_4}. \tag{51}$$

We next proceed to estimate the terms $\mathfrak{T}_1,\cdots,\mathfrak{T}_4$.

(iii.A) *Estimate of* $\mathfrak{T}_1$. For the term $\mathfrak{T}_1$, we add $\pm\boldsymbol{\pi}_T^0\boldsymbol{w}$ in the third factor, so we have that

$$\begin{aligned}\mathfrak{T}_1 &= \sum_{T\in\mathcal{T}_h}\int_T (\boldsymbol{G}_T^{2(k+1)}\underline{\hat{\boldsymbol{w}}}_T - \nabla\boldsymbol{w})\boldsymbol{R}_T^k\underline{\boldsymbol{z}}_T\cdot(\boldsymbol{w}-\boldsymbol{\pi}_T^0\boldsymbol{w}) + \sum_{T\in\mathcal{T}_h}\int_T (\boldsymbol{G}_T^{2(k+1)}\underline{\hat{\boldsymbol{w}}}_T - \nabla\boldsymbol{w})\boldsymbol{R}_T^k\underline{\boldsymbol{z}}_T\cdot\boldsymbol{\pi}_T^0\boldsymbol{w}\\ &=: \mathfrak{T}_{1,1}+\mathfrak{T}_{1,2}.\end{aligned}$$

To bound $\mathfrak{T}_{1,1}$, we use Hölder inequalities with exponents $(2,4,4)$, the approximation properties (32) of $\boldsymbol{G}_T^{2(k+1)}$ with $l=2(k+1)$ and $m=k+1$, and (13a) of the L^2-projector with $l=0$, $m=0$, $r=4$, and $s=1$, so it holds that

$$\begin{aligned}|\mathfrak{T}_{1,1}| &\lesssim \sum_{T\in\mathcal{T}_h}\|\boldsymbol{G}_T^{2(k+1)}\underline{\hat{\boldsymbol{w}}}_T - \nabla\boldsymbol{w}\|_{L^2(T)^{3\times3}}\|\boldsymbol{R}_T^k\underline{\boldsymbol{z}}_T\|_{L^4(T)^3}\|\boldsymbol{w}-\boldsymbol{\pi}_T^0\boldsymbol{w}\|_{L^4(T)^3}\\ &\lesssim h^{k+1}|\boldsymbol{w}|_{H^{k+1}(\mathcal{T}_h)^3}\|\boldsymbol{R}_h^k\underline{\boldsymbol{z}}_h\|_{L^4(\Omega)^3}|\boldsymbol{w}|_{W^{1,4}(\Omega)^3}\\ &\lesssim h^{k+1}|\boldsymbol{w}|_{H^{k+1}(\mathcal{T}_h)^3}\|\underline{\boldsymbol{z}}_T\|_{1,h}|\boldsymbol{w}|_{W^{1,4}(\Omega)^3},\end{aligned} \tag{52}$$

where, in the last step, we have used the discrete Sobolev embedding (22) with $r=4$ and recalled that the assumed regularity implies $\boldsymbol{w}\in W^{1,4}(\Omega)^3$.

For $\mathfrak{T}_{1,2}$, we start by observing that

$$\mathfrak{T}_{1,2} = \sum_{T\in\mathcal{T}_h}\int_T (\boldsymbol{G}_T^{2(k+1)}\underline{\hat{\boldsymbol{w}}}_T - \nabla\boldsymbol{w}) : \boldsymbol{\pi}_T^0\boldsymbol{w}\otimes\boldsymbol{R}_T^k\underline{\boldsymbol{z}}_T.$$

Integrating by parts the term involving $\nabla\boldsymbol{w}$ and using, for each element $T\in\mathcal{T}_h$, the definition (30) of $\boldsymbol{G}_T^{2(k+1)}$ with $\underline{\boldsymbol{v}}_T=\underline{\hat{\boldsymbol{w}}}_T$ and $\boldsymbol{\tau}=\boldsymbol{\pi}_T^0\boldsymbol{w}\otimes\boldsymbol{R}_T^k\underline{\boldsymbol{z}}_T$ (this is possible since $\boldsymbol{\pi}_T^0\boldsymbol{w}\otimes\boldsymbol{R}_T^k\underline{\boldsymbol{z}}_T\in\mathbb{P}^{k+1}(T)^{3\times3}\subset\mathbb{P}^{2(k+1)}(T)^{3\times3}$), we get

$$\mathfrak{T}_{1,2} = -\sum_{T\in\mathcal{T}_h}\int_T(\boldsymbol{\pi}_T^k\boldsymbol{w}-\boldsymbol{w})\cdot\nabla\cdot(\boldsymbol{\pi}_T^0\boldsymbol{w}\otimes\boldsymbol{R}_T^k\underline{\boldsymbol{z}}_T) + \sum_{T\in\mathcal{T}_h}\sum_{F\in\mathcal{F}_T}\int_F(\boldsymbol{\pi}_F^k\boldsymbol{w}-\boldsymbol{w})\cdot(\boldsymbol{\pi}_T^0\boldsymbol{w}\otimes\boldsymbol{R}_T^k\underline{\boldsymbol{z}}_T\boldsymbol{n}_{TF}). \tag{53}$$

We have $\nabla\cdot(\boldsymbol{\pi}_T^0\boldsymbol{w}\otimes\boldsymbol{R}_T^k\underline{\boldsymbol{z}}_T) = \boldsymbol{\pi}_T^0\boldsymbol{w}(\nabla\cdot\boldsymbol{R}_T^k\underline{\boldsymbol{z}}_T)\in\mathbb{P}^k(T)^3$. Then, recalling the definition (12) of $\boldsymbol{\pi}_T^k$, the first term of the right hand side of (53) vanishes. Moreover, $\boldsymbol{\pi}_T^0\boldsymbol{w}\otimes\boldsymbol{R}_T^k\underline{\boldsymbol{z}}_T\boldsymbol{n}_{TF} = \boldsymbol{\pi}_T^0\boldsymbol{w}(\boldsymbol{R}_T^k\underline{\boldsymbol{z}}_T\cdot\boldsymbol{n}_{TF})\in\mathbb{P}^k(F)^3$ (see (20b)). Then, by definition (12) of $\boldsymbol{\pi}_F^k$, the second term of the right hand side of (53) vanishes as well, giving

$$\mathfrak{T}_{1,2} = 0.$$

Combining this result with (52), we conclude that

$$|\mathfrak{T}_1| \le h^{k+1}|\boldsymbol{w}|_{H^{k+1}(\mathcal{T}_h)^3}\|\underline{\boldsymbol{z}}_T\|_{1,h}|\boldsymbol{w}|_{W^{1,4}(\Omega)^3}. \tag{54}$$

(iii.B) *Estimate of* $\mathfrak{T}_2$. For the term $\mathfrak{T}_2$ in (51), we insert $\pm\boldsymbol{\pi}_T^0\boldsymbol{w}$ into the second factor, so we can write

$$\begin{aligned}\mathfrak{T}_2 &= \sum_{T\in\mathcal{T}_h}\int_T(\nabla\boldsymbol{w}-\boldsymbol{G}_T^{2(k+1)}\hat{\underline{\boldsymbol{w}}}_T)(\boldsymbol{w}-\boldsymbol{\pi}_T^0\boldsymbol{w})\cdot\boldsymbol{R}_T^k\underline{\boldsymbol{z}}_T+\sum_{T\in\mathcal{T}_h}\int_T(\nabla\boldsymbol{w}-\boldsymbol{G}_T^{2(k+1)}\hat{\underline{\boldsymbol{w}}}_T)\boldsymbol{\pi}_T^0\boldsymbol{w}\cdot\boldsymbol{R}_T^k\underline{\boldsymbol{z}}_T\\ &=: \mathfrak{T}_{2,1}+\mathfrak{T}_{2,2}.\end{aligned}\tag{55}$$

We bound $\mathfrak{T}_{2,1}$ similarly as done with $\mathfrak{T}_{1,1}$ in (52), that is, we use Hölder inequalities with exponents $(2,4,4)$, the approximation properties of $\boldsymbol{G}_T^{2(k+1)}$ and $\boldsymbol{\pi}_T^0$, and (22) with $r=4$, so it is inferred that

$$|\mathfrak{T}_{2,1}|\lesssim h^{k+1}|\boldsymbol{w}|_{H^{k+1}(\mathcal{T}_h)^3}|\boldsymbol{w}|_{W^{1,4}(\Omega)^3}\|\underline{\boldsymbol{z}}_T\|_{1,h}.\tag{56}$$

To estimate $\mathfrak{T}_{2,2}$ in (55), we integrate by parts the term involving $\nabla\boldsymbol{w}$ and we use, for each element $T\in\mathcal{T}_h$, the definition (30) of $\boldsymbol{G}_T^{2(k+1)}$ with $\underline{\boldsymbol{v}}_T=\hat{\underline{\boldsymbol{w}}}_T$ and $\boldsymbol{\tau}=\boldsymbol{R}_T^k\underline{\boldsymbol{z}}_T\otimes\boldsymbol{\pi}_T^0\boldsymbol{w}$ (this is possible since $\boldsymbol{R}_T^k\underline{\boldsymbol{z}}_T\otimes\boldsymbol{\pi}_T^0\boldsymbol{w}\in\mathbb{P}^{k+1}(T)^{3\times3}\subset\mathbb{P}^{2(k+1)}(T)^{3\times3}$) to write

$$\mathfrak{T}_{2,2}=-\sum_{T\in\mathcal{T}_h}\cancel{\int_T(\boldsymbol{w}-\boldsymbol{\pi}_T^k\boldsymbol{w})\cdot\nabla\cdot(\boldsymbol{R}_T^k\underline{\boldsymbol{z}}_T\otimes\boldsymbol{\pi}_T^0\boldsymbol{w})}+\sum_{T\in\mathcal{T}_h}\sum_{F\in\mathcal{F}_T}\int_F(\boldsymbol{w}-\boldsymbol{\pi}_F^k\boldsymbol{w})\cdot(\boldsymbol{R}_T^k\underline{\boldsymbol{z}}_T\otimes\boldsymbol{\pi}_T^0\boldsymbol{w})\boldsymbol{n}_{TF},\tag{57}$$

where we have cancelled the first integral in (57) observing that

$$\nabla\cdot(\boldsymbol{R}_T^k\underline{\boldsymbol{z}}_T\otimes\boldsymbol{\pi}_T^0\boldsymbol{w})=\nabla\boldsymbol{R}_T^k\underline{\boldsymbol{z}}_T\boldsymbol{\pi}_T^0\boldsymbol{w}+\cancel{\boldsymbol{R}_T^k\underline{\boldsymbol{z}}_T(\nabla\cdot\boldsymbol{\pi}_T^0\boldsymbol{w})}\in\mathbb{P}^k(T)^3,$$

and using the definition (12) of $\boldsymbol{\pi}_T^k$. To bound the second term in (57), we add the quantity $\pm\boldsymbol{\pi}_T^0\boldsymbol{R}_T^k\underline{\boldsymbol{z}}_T$ in its second factor, so we get that

$$\begin{aligned}\int_F(\boldsymbol{w}-\boldsymbol{\pi}_F^k\boldsymbol{w})\cdot(\boldsymbol{R}_T^k\underline{\boldsymbol{z}}_T\otimes\boldsymbol{\pi}_T^0\boldsymbol{w})\boldsymbol{n}_{TF}&=\int_F(\boldsymbol{w}-\boldsymbol{\pi}_F^k\boldsymbol{w})\cdot\left[(\boldsymbol{R}_T^k\underline{\boldsymbol{z}}_T-\boldsymbol{\pi}_T^0\boldsymbol{R}_T^k\underline{\boldsymbol{z}}_T)\otimes\boldsymbol{\pi}_T^0\boldsymbol{w}\right]\boldsymbol{n}_{TF}\\&\quad+\cancel{\int_F(\boldsymbol{w}-\boldsymbol{\pi}_F^k\boldsymbol{w})\cdot(\boldsymbol{\pi}_T^0\boldsymbol{R}_T^k\underline{\boldsymbol{z}}_T\otimes\boldsymbol{\pi}_T^0\boldsymbol{w})\boldsymbol{n}_{TF}},\end{aligned}\tag{58}$$

where we have cancelled the second integral of the right hand side of (58) using the definition (12) of $\boldsymbol{\pi}_F^k$ after observing that $(\boldsymbol{\pi}_T^0\boldsymbol{R}_T^k\underline{\boldsymbol{z}}_T\otimes\boldsymbol{\pi}_T^0\boldsymbol{w})_{|F}\boldsymbol{n}_{TF}\in\mathbb{P}^0(F)^3\subset\mathbb{P}^k(F)^3$. So, plugging (58) into (57) and applying Hölder inequalities with exponents $(4,2,4,\infty)$ along with $\|\boldsymbol{n}_{TF}\|_{L^\infty(F)^3}=1$, we can write

$$|\mathfrak{T}_{2,2}|\le\sum_{T\in\mathcal{T}_h}\sum_{F\in\mathcal{F}_T}\|\boldsymbol{w}-\boldsymbol{\pi}_F^k\boldsymbol{w}\|_{L^4(F)^3}\|\boldsymbol{R}_T^k\underline{\boldsymbol{z}}_T-\boldsymbol{\pi}_T^0\boldsymbol{R}_T^k\underline{\boldsymbol{z}}_T\|_{L^2(F)^3}\|\boldsymbol{\pi}_T^0\boldsymbol{w}\|_{L^4(F)^3}.\tag{59}$$

To estimate the first term in (59), we add $\pm\boldsymbol{\pi}_T^k\boldsymbol{w}$, so we can write

$$\begin{aligned}\|\boldsymbol{w}-\boldsymbol{\pi}_F^k\boldsymbol{w}\|_{L^4(F)^3}&\le\|\boldsymbol{\pi}_T^k\boldsymbol{w}-\boldsymbol{\pi}_F^k\boldsymbol{w}\|_{L^4(F)^3}+\|\boldsymbol{w}-\boldsymbol{\pi}_T^k\boldsymbol{w}\|_{L^4(F)^3}\\&\le\|\boldsymbol{\pi}_F^k(\boldsymbol{\pi}_T^k\boldsymbol{w}-\boldsymbol{w})\|_{L^4(F)^3}+\|\boldsymbol{w}-\boldsymbol{\pi}_T^k\boldsymbol{w}\|_{L^4(F)^3}\lesssim\|\boldsymbol{w}-\boldsymbol{\pi}_T^k\boldsymbol{w}\|_{L^4(F)^3},\end{aligned}$$

where, in the last line, we have used the L^4-boundedness of $\boldsymbol{\pi}_F^k$ (see [20, Lemma 3.2]). Thus, using this last inequality in (59), we get

$$\begin{aligned}|\mathfrak{T}_{2,2}|&\lesssim\sum_{T\in\mathcal{T}_h}\sum_{F\in\mathcal{F}_T}\|\boldsymbol{w}-\boldsymbol{\pi}_T^k\boldsymbol{w}\|_{L^4(F)^3}\|\boldsymbol{R}_T^k\underline{\boldsymbol{z}}_T-\boldsymbol{\pi}_T^0\boldsymbol{R}_T^k\underline{\boldsymbol{z}}_T\|_{L^2(F)^3}\|\boldsymbol{\pi}_T^0\boldsymbol{w}\|_{L^4(F)^3}\\&\lesssim\sum_{T\in\mathcal{T}_h}h_T^{k+1}|\boldsymbol{w}|_{W^{k+1,4}(T)^3}|\boldsymbol{R}_T^k\underline{\boldsymbol{z}}_T|_{H^1(T)^3}\|\boldsymbol{w}\|_{W^{1,4}(T)^3}.\end{aligned}\tag{60}$$

To pass from the first to the second line, we have used the approximation properties (13b) of the L^2-orthogonal projector, with $l = k$, $m = 0$, $r = 4$, and $s = k+1$ for the first factor and with $m = 0$, $r = 2$, and $s = 1$ for the second factor. For the third factor, we have used the L^4-boundedness of $\boldsymbol{\pi}_T^0$ and a local trace inequality (see, e.g., [20, Eq. (A.10)]) together with $h_T \le h_\Omega \lesssim 1$ to write $\|\boldsymbol{\pi}_T^0 \boldsymbol{w}\|_{L^4(F)^3} \lesssim \|\boldsymbol{w}\|_{L^4(F)^3} \lesssim h_T^{-\frac{1}{4}} \|\boldsymbol{w}\|_{W^{1,4}(T)^3}$. To further bound the second factor in (60), observe that we can write

$$|\boldsymbol{R}_T^k \underline{\boldsymbol{z}}_T|_{H^1(T)^3} \le |\boldsymbol{R}_T^k \underline{\boldsymbol{z}}_T - \boldsymbol{z}_T|_{H^1(T)^3} + |\boldsymbol{z}_T|_{H^1(T)^3}. \tag{61}$$

For the first term in the right-hand side, we can proceed to write

$$|\boldsymbol{R}_T^k \underline{\boldsymbol{z}}_T - \boldsymbol{z}_T|_{H^1(T)^3} \lesssim h_T^{-1} \|\boldsymbol{R}_T^k \underline{\boldsymbol{z}}_T - \boldsymbol{z}_T\|_{L^2(T)^3} \lesssim |\underline{\boldsymbol{z}}_T|_{1,\partial T},$$

where we have used the uniform local inverse inequality $\|\nabla v\|_{L^2(T)^3} \lesssim h_T^{-1} \|v\|_{L^2(T)}$ valid for any polynomial function v and the bound (21) in the second inequality. Thus, plugging the above inequality into (61) and recalling the definition (15) of the $\|\cdot\|_{1,T}$ seminorm, we get

$$|\boldsymbol{R}_T^k \underline{\boldsymbol{z}}_T|_{H^1(T)^3} \lesssim \|\underline{\boldsymbol{z}}_T\|_{1,T}.$$

Plugging the above bound into (60), using a discrete Hölder inequality with exponents $(4, 2, 4)$ on the sum over $T \in \mathcal{T}_h$, and recalling the definition (14) of the $\|\cdot\|_{1,h}$-norm, we arrive at

$$|\mathfrak{T}_{2,2}| \lesssim h^{k+1} |\boldsymbol{w}|_{W^{k+1,4}(\mathcal{T}_h)^3} \|\underline{\boldsymbol{z}}_T\|_{1,h} \|\boldsymbol{w}\|_{W^{1,4}(\Omega)^3}.$$

Combining this estimate with (56), we finally bound (55) as

$$|\mathfrak{T}_2| \lesssim h^{k+1} |\boldsymbol{w}|_{W^{k+1,4}(\mathcal{T}_h)^3} \|\boldsymbol{w}\|_{W^{1,4}(\Omega)^3} \|\underline{\boldsymbol{z}}_T\|_{1,h}. \tag{62}$$

(iii.C) *Estimate of* $\mathfrak{T}_3$ *and* $\mathfrak{T}_4$. Moving to $\mathfrak{T}_3$, we use continuous Hölder inequalities with exponents $(2, 4, 4)$, the boundedness (31) of $\boldsymbol{G}_T^{2(k+1)}$ and (16) of $\underline{\boldsymbol{I}}_h^k$ to infer, for all $T \in \mathcal{T}_h$,

$$\|\boldsymbol{G}_T^{2(k+1)} \underline{\hat{\boldsymbol{w}}}_T\|_{L^2(T)^{3\times 3}} \lesssim |\boldsymbol{w}|_{H^1(T)^3},$$

discrete Hölder inequalities on the sum over $T \in \mathcal{T}_h$ with exponents $(2, 4, 4)$, and the Sobolev inequality (22) with $r = 4$ to obtain

$$|\mathfrak{T}_3| \lesssim |\boldsymbol{w}|_{H^1(\Omega)^3} \left(\sum_{T\in\mathcal{T}_h} \|\boldsymbol{w} - \boldsymbol{R}_T^k \underline{\hat{\boldsymbol{w}}}_T\|_{L^4(T)^3}^4 \right)^{\frac{1}{4}} \|\underline{\boldsymbol{z}}_h\|_{1,h}.$$

To bound the addends in the second factor, recall that $\boldsymbol{R}_T^k \underline{\hat{\boldsymbol{w}}}_T = \boldsymbol{R}_T^k \underline{\boldsymbol{I}}_T^k \boldsymbol{w} = \boldsymbol{I}_{\mathbb{RTN},T}^k \boldsymbol{w}$ and use the approximation results of [24, Lemma 3.17] to write, for all $T \in \mathcal{T}_h$,

$$\|\boldsymbol{w} - \boldsymbol{I}_{\mathbb{RTN},T}^k \boldsymbol{w}\|_{L^4(T)^3} \lesssim h_T^{k+1} |\boldsymbol{w}|_{W^{k+1,4}(T)^3}.$$

In conclusion, we have that

$$|\mathfrak{T}_3| \lesssim h^{k+1} |\boldsymbol{w}|_{H^1(\Omega)^3} |\boldsymbol{w}|_{W^{k+1,4}(\mathcal{T}_h)^3} \|\underline{\boldsymbol{z}}_T\|_{1,h}. \tag{63}$$

Using similar arguments as for $\mathfrak{T}_3$, we have for the last term

$$|\mathfrak{T}_4| \lesssim h^{k+1} |\boldsymbol{w}|_{H^1(\Omega)^3} \|\underline{\boldsymbol{z}}_T\|_{1,h} |\boldsymbol{w}|_{W^{k+1,4}(\mathcal{T}_h)^3}. \tag{64}$$

(iii.D) *Conclusion.* Taking absolute values in (51), recalling the definition (19) of the dual norm, and invoking the estimates (54), (62), (63), and (64), the conclusion follows. □

4.5 Discrete problem

The HHO discretization of problem (1) then reads: Find $(\underline{\boldsymbol{u}}_h, p_h) \in \underline{\boldsymbol{U}}_{h,0}^k \times P_h^k$ such that

$$\nu a_h(\underline{\boldsymbol{u}}_h, \underline{\boldsymbol{v}}_h) + t_h(\underline{\boldsymbol{u}}_h, \underline{\boldsymbol{u}}_h, \underline{\boldsymbol{v}}_h) + b_h(\underline{\boldsymbol{v}}_h, p_h) = \ell_h(\boldsymbol{f}, \underline{\boldsymbol{v}}_h) \quad \forall \underline{\boldsymbol{v}}_h \in \underline{\boldsymbol{U}}_{h,0}, \tag{65a}$$

$$-b_h(\underline{\boldsymbol{u}}_h, q_h) = 0 \quad \forall q_h \in \mathbb{P}^k(\mathcal{T}_h). \tag{65b}$$

The existence of a solution to (65) for any $\boldsymbol{f} \in L^2(\Omega)^3$ can be proved using a topological degree argument as in [21, Theorem 1]. Similarly, uniqueness can be proved along the lines of Theorem 2 therein under a smallness condition on $\boldsymbol{e}2f$. These arguments will not be repeated here for the sake of conciseness, and we will limit ourselves to proving the discrete counterpart of the uniform a priori bound (11) on the velocity, which will be needed in the convergence analysis.

Proposition 8 (Uniform a priori bound on the discrete velocity)**.** *Let $(\underline{\boldsymbol{u}}_h, p_h) \in \underline{\boldsymbol{U}}_{h,0}^k \times P_h^k$ be a solution to (65). Then, recalling the Hodge decomposition (4) of $\boldsymbol{f}$, we have the following uniform a priori bound for the velocity:*

$$\|\underline{\boldsymbol{u}}_h\|_{1,h} \lesssim \nu^{-1} \|\boldsymbol{g}\|_{L^2(\Omega)^3}. \tag{66}$$

Proof. We use similar arguments as for the continuous problem; see Section 2.3. Taking $\underline{\boldsymbol{v}}_h = \underline{\boldsymbol{u}}_h$ in (65a), $q_h = p_h - \lambda \pi_h^k \psi$ in (65b), and summing the resulting relations, we get

$$\nu a_h(\underline{\boldsymbol{u}}_h, \underline{\boldsymbol{u}}_h) + t_h(\underline{\boldsymbol{u}}_h, \underline{\boldsymbol{u}}_h, \underline{\boldsymbol{u}}_h) + b_h(\underline{\boldsymbol{u}}_h, p_h) - b_h(\underline{\boldsymbol{u}}_h, p_h - \lambda \pi_h^k \psi)$$
$$= \ell_h(\boldsymbol{f}, \underline{\boldsymbol{v}}_h) = \ell_h(\boldsymbol{g}, \underline{\boldsymbol{u}}_h) + b_h(\underline{\boldsymbol{u}}_h, \lambda \pi_h^k \psi),$$

where we have used the discrete velocity invariance property (41) to conclude. Simplifying the terms involving the bilinear form b_h in the above expression, invoking the non-dissipativity property (46) to write $t_h(\underline{\boldsymbol{u}}_h, \underline{\boldsymbol{u}}_h, \underline{\boldsymbol{u}}_h) = 0$, we arrive at

$$\nu a_h(\underline{\boldsymbol{u}}_h, \underline{\boldsymbol{u}}_h) = \ell_h(\boldsymbol{g}, \underline{u}_h).$$

Using the stability of a_h expressed by the first inequality in (34) in the left-hand side along with the Cauchy–Schwarz and discrete Poincaré inequalities (the latter corresponding to (22) with $r = 2$) in the right-hand side, we get

$$\nu C_a \|\underline{\boldsymbol{u}}_h\|_{1,h}^2 \le \nu a_h(\underline{\boldsymbol{u}}_h, \underline{\boldsymbol{u}}_h) = \ell_h(\boldsymbol{g}, \underline{\boldsymbol{u}}_h) \le \|\boldsymbol{g}\|_{L^2(\Omega)^3} \|\boldsymbol{R}_h^k \underline{\boldsymbol{u}}_h\|_{L^2(\Omega)^3} \le \|\boldsymbol{g}\|_{L^2(\Omega)^3} \|\underline{\boldsymbol{u}}_h\|_{1,h}.$$

Simplifying by $\|\underline{\boldsymbol{u}}_h\|_{1,h}$ yields the desired result. □

Remark 9 (Efficient implementation). When solving the system of nonlinear algebraic equations corresponding to (65) by a first-order algorithm, all element-based velocity unknowns and all but one pressure unknowns per element can be statically condensed as described for the Stokes problem in [19, Section 6.2]. As a result, after strongly enforcing the Dirichlet boundary condition on the velocity, we end up solving at each iteration a linear system of size

$$d \operatorname{card}(\mathcal{F}_h^{\mathrm{i}}) \binom{k+d-1}{d-1} + \operatorname{card}(\mathcal{T}_h).$$

Notice that the presence of the velocity reconstruction $\boldsymbol{R}_h^k$ in the right-hand side of (65a) slightly modifies the static condensation procedure with respect to the one described in [19, Section 6] in that, comparing with Eq. (47) therein, the linearised convective term appears in the left-hand side, while the first term in the right-hand side has a nonzero second component (reflecting the fact that also face unknowns are used to discretise the body force).

Remark 10 (The two-dimensional case). The two-dimensional version of the method (65) will be considered numerically in Section 6. Denoting by u_i, $i = 1, \ldots, 3$, the component of the velocity field along the Cartesian axis x_i, the two-dimensional plane velocity problem can be recovered from (1) setting $u_3 = 0$ and assuming that u_1 and u_2 do not depend on x_3. In practice, the expression (45) of the discrete trilinear form naturally lends itself to two-dimensional implementations, since we have removed the (inherently three-dimensional) curl operator exploiting Proposition 1.

5 Convergence analysis

We estimate the error defined as the difference between the solution to the HHO scheme and the interpolate of the exact solution, denoted by

$$(\hat{\underline{\boldsymbol{u}}}_h, \hat{p}_h) \coloneqq (\underline{\boldsymbol{I}}_h^k \boldsymbol{u}, \pi_h^k p) \in \underline{\boldsymbol{U}}_{h,0}^k \times P_h^k. \tag{67}$$

Theorem 11 (Error estimate for small data)**.** *Recalling the Hodge decomposition (4) of the forcing term $\boldsymbol{f}$, we assume that it holds, for some $\alpha \in (0,1)$,*

$$\|\boldsymbol{g}\|_{L^2(\Omega)^3} \le \alpha \frac{\nu^2 C_a}{C_t C_I C_P}, \tag{68}$$

where C_a, C_t, and C_I are defined in (34), (47) and (16), respectively, while C_P is the continuous Poincaré constant appearing in (11). Let $(\boldsymbol{u}, p) \in \boldsymbol{U} \times P$ and $(\underline{\boldsymbol{u}}_h, p_h) \in \underline{\boldsymbol{U}}_h^k \times P_h^k$ solve (1) and (65), respectively. Assume the additional regularity $\boldsymbol{u} \in H^{k+2}(\mathcal{T}_h)^3$ and $p \in H^1(\Omega) \cap H^{k+1}(\mathcal{T}_h)$, and let $(\hat{\underline{\boldsymbol{u}}}_h, \hat{p}_h)$ be defined by (67). Then, it holds:

$$\|\underline{\boldsymbol{u}}_h - \hat{\underline{\boldsymbol{u}}}_h\|_{1,h} + \nu^{-1}\|p_h - \hat{p}_h\|_{L^2(\Omega)} \lesssim h^{k+1}(1-\alpha)^{-1}\left(|\boldsymbol{u}|_{H^{k+2}(\mathcal{T}_h)^3} + \nu^{-1}\|\boldsymbol{u}\|_{W^{1,4}(\Omega)^3}|\boldsymbol{u}|_{W^{k+1,4}(\mathcal{T}_h)^3}\right). \tag{69}$$

where the hidden constant is independent of ν, λ, h as well as $(\boldsymbol{u}, p)$.

Before proving Theorem 11, some remarks are in order.

Remark 12 (Robustness with respect to irrotational body forces). Crucially, the error estimate in Theorem 11:

(i) is established under a data smallness condition which only involves the solenoidal part of the body force, and is thus valid for arbitrary λ in (4);

(ii) is uniform in λ, meaning that the right-hand side is independent of this parameter and of the pressure. The latter point is crucial since, recalling Remark 2, one cannot expect that the pressure remains bounded as $\lambda \to \infty$.

These properties are obtained without requiring an explicit (exact or approximate) knowledge of the Hodge decomposition (4) of the body force. Instead, they result from the careful design of the discretizations of the body force itself and of the convective term. In both cases, a key role is played by the $\boldsymbol{H}(\mathrm{div};\Omega)$-conforming velocity reconstruction of Section 3.4.

Remark 13 (Comparison with the exact solution). Starting from (69) and proceeding as in [21, Corollary 16], one can derive the following error estimates that explicitly compare the discrete and exact solutions:

$$\|\boldsymbol{G}_h^k \underline{\boldsymbol{u}}_h - \nabla \boldsymbol{u}\|_{L^2(\Omega)^{3\times 3}} \lesssim h^{k+1}(1-\alpha)^{-1}\left(|\boldsymbol{u}|_{H^{k+2}(\mathcal{T}_h)^3} + \nu^{-1}\|\boldsymbol{u}\|_{W^{1,4}(\Omega)^3}|\boldsymbol{u}|_{W^{k+1,4}(\mathcal{T}_h)^3}\right) \tag{70}$$

and

$$\|p_h - p\|_{L^2(\Omega)} \lesssim h^{k+1}\frac{1+\nu}{1-\alpha}\left(|\boldsymbol{u}|_{H^{k+2}(\mathcal{T}_h)^3} + \nu^{-1}\|\boldsymbol{u}\|_{W^{1,4}(\Omega)^3}|\boldsymbol{u}|_{W^{k+1,4}(\mathcal{T}_h)^3} + |p|_{H^{k+1}(\mathcal{T}_h)}\right). \tag{71}$$

Notice that the estimate (70) on the velocity remains uniform in λ, while a dependence on λ appears in the estimate (71) for the pressure through the term $|p|_{H^{k+1}(\mathcal{T}_h)}$ (see Remark 2).

Remark 14 (Comparison with divergence-free Hybridisable Discontinuous Galerkin methods). It has been shown in [14] that HHO methods are intimately linked to Hybridisable Discontinuous Galerkin (HDG) methods, which therefore deserve a more in-depth discussion. In this context we will focus, in particular, on divergence-free HDG methods.

In [9], the authors propose a two-dimensional divergence-free HDG method based on approximations of degree $(k-1)$ of the vorticity inside elements and of degree k of the velocity inside each element and at mesh edges. Error estimates in h^k (as opposed to h^{k+1} for the present method, which is valid both in two and three space dimensions) are proved. The right-hand side of the velocity error estimate of [9, Theorem 4.1] is independent of the pressure, which seems to indicate that the method can achieve robustness with respect to irrotational body forces, although this property is not explicitly brought up in the discussion.

In [10], the authors consider an HDG method based on polynomial approximations of total degree $\leq k$ of the velocity gradient at elements, of the velocity at elements and faces, and of the pressure at elements. Convergence in h^{k+1} for the L^2-norm of each variable is proved for a suitable choice of the penalty parameter, and a divergence-free velocity post-processing is also proposed. Contrary to (70), the right-hand side of the estimate on the velocity given in [10, Theorem 2.4] depends on the pressure, indicating a potential lack of robustness with respect to large irrotational body forces, i.e., for $\lambda \to \infty$. This is possibly due to the fact that the discretisation of the convective term and of the body force do not make use of a divergence-free test function, showing that methods that yield globally divergence free velocity approximation are not necessarily robust. Indeed, the main takeaway message of the present work is that, in order to achieve robustness with respect to irrotational body forcees, divergence-free test functions should be used in the discretisation of the body force, of the convective term and, in the unsteady case, of the time derivative. When the global divergence-free property for the discrete velocity is enforced through Lagrange multipliers, the test functions in these terms should be replaced by their projection on a $\mathbf{H}(\mathrm{div};\Omega)$-conforming space, which is precisely the idea underlying the velocity reconstruction of Section 3.4 and the formulations of Sections 4.3 (body force) and (4.4) (convective term).

In [33], the authors consider an HDG method with velocity unknowns that, for any integer $k \geq 1$, are polynomials of degree k inside each element and $(k-1)$ on each face. This choice, combined with the stabilisation of [32, 39], delivers convergence in h^k for both the velocity energy norm and the pressure L^2-norm. In contrast with the present work which gives a formal proof, the method presented in [33] is only numerically evaluated, and it is unclear whether a robust behaviour with respect to large irrotational body forces can be expected or not.

More recently, a divergence-free HDG method has been presented in [43], for which a pressure-robustness property is numerically demonstrated; cf., in particular, Section 4.3 therein. Given an integer $k \geq 1$, the HDG method hinges, in this case, on approximations of the velocity at elements and faces of degree k, and of the pressure at elements of degree $(k-1)$, and at faces of degree k (in the present method, pressure unknowns of degree k at element are considered, with only one pressure degree of freedom per element remaining after static condensation; cf. Remark 9; our method therefore gives a reduced computational cost, since produces fewer unknowns). The numerical results show a convegence in h^{k+1} and h^k for the L^2-norms of the velocity and of the pressure, respectively. This method also constitutes an improvement of previous works [31, 42] in that it conserves locally both the mass and the momentum.

Proof of Theorem 11. (i) *Estimate on the velocity.* Set $(\underline{\boldsymbol{e}}_h, \epsilon_h) \coloneqq (\underline{\boldsymbol{u}}_h - \underline{\hat{\boldsymbol{u}}}_h, p_h - \hat{p}_h)$ and define the consistency error linear form $\mathcal{E}_h : \underline{\boldsymbol{U}}_h^k \to \mathbb{R}$ such that, for all $\underline{\boldsymbol{v}}_h \in \underline{\boldsymbol{U}}_{h,0}^k$,

$$\mathcal{E}_h(\underline{\boldsymbol{v}}_h) \coloneqq \ell_h(\boldsymbol{f}, \underline{\boldsymbol{v}}_h) - \nu a_h(\underline{\hat{\boldsymbol{u}}}_h, \underline{\boldsymbol{v}}_h) - t_h(\underline{\hat{\boldsymbol{u}}}_h, \underline{\hat{\boldsymbol{u}}}_h, \underline{\boldsymbol{v}}_h) - b_h(\underline{\boldsymbol{v}}_h, \hat{p}_h). \tag{72}$$

We next proceed to establish a stability property and an upper bound for $\mathcal{E}_h$.

(i.A) *Stability.* Substituting $\ell_h(\boldsymbol{f}, \underline{\boldsymbol{v}}_h)$ from (65a) in (72), we get

$$\mathcal{E}_h(\underline{\boldsymbol{v}}_h) = \nu a_h(\underline{\boldsymbol{e}}_h, \underline{\boldsymbol{v}}_h) + t_h(\underline{\boldsymbol{u}}_h, \underline{\boldsymbol{u}}_h, \underline{\boldsymbol{v}}_h) - t_h(\underline{\hat{\boldsymbol{u}}}_h, \underline{\hat{\boldsymbol{u}}}_h, \underline{\boldsymbol{v}}_h) + b_h(\underline{\boldsymbol{v}}_h, \epsilon_h). \tag{73}$$

Choose $\underline{\boldsymbol{v}}_h = \underline{\boldsymbol{e}}_h$. Using the skew-symmetry (46) of t_h together with linearity in its second argument yields

$$0 = t_h(\underline{\boldsymbol{u}}_h, \underline{\boldsymbol{e}}_h, \underline{\boldsymbol{e}}_h) = t_h(\underline{\boldsymbol{u}}_h, \underline{\boldsymbol{u}}_h, \underline{\boldsymbol{e}}_h) - t_h(\underline{\boldsymbol{u}}_h, \underline{\hat{\boldsymbol{u}}}_h, \underline{\boldsymbol{e}}_h)$$

and then, using its boundedness (47),

$$\begin{aligned} |t_h(\underline{\boldsymbol{u}}_h, \underline{\boldsymbol{u}}_h, \underline{\boldsymbol{e}}_h) - t_h(\underline{\hat{\boldsymbol{u}}}_h, \underline{\hat{\boldsymbol{u}}}_h, \underline{\boldsymbol{e}}_h)| &= |t_h(\underline{\boldsymbol{u}}_h, \underline{\hat{\boldsymbol{u}}}_h, \underline{\boldsymbol{e}}_h) - t_h(\underline{\hat{\boldsymbol{u}}}_h, \underline{\hat{\boldsymbol{u}}}_h, \underline{\boldsymbol{e}}_h)| \\ &= |t_h(\underline{\boldsymbol{e}}_h, \underline{\hat{\boldsymbol{u}}}_h, \underline{\boldsymbol{e}}_h)| \le C_t \|\underline{\boldsymbol{e}}_h\|_{1,h}^2 \|\underline{\hat{\boldsymbol{u}}}_h\|_{1,h}. \end{aligned}$$

By (65b) and (38) with $q_h = \epsilon_h$ along with (1b) with $q = \epsilon_h$, it is readily inferred that

$$b_h(\underline{\boldsymbol{e}}_h, \epsilon_h) = 0.$$

Therefore, returning to (73) with $\underline{\boldsymbol{v}}_h = \underline{\boldsymbol{e}}_h$ and using the coercivity (34) of a_h,

$$\begin{aligned} \mathcal{E}_h(\underline{\boldsymbol{e}}_h) &\ge \left(\nu C_a - C_t \|\underline{\hat{\boldsymbol{u}}}_h\|_{1,h}\right) \|\underline{\boldsymbol{e}}_h\|_{1,h}^2 \\ &\ge \left(\nu C_a - \nu^{-1} C_t C_I C_P \|\boldsymbol{g}\|_{L^2(\Omega)^3}\right) \|\underline{\boldsymbol{e}}_h\|_{1,h}^2 \ge (1-\alpha)\nu C_a \|\underline{\boldsymbol{e}}_h\|_{1,h}^2, \end{aligned} \tag{74}$$

where, to pass to the second line, we have used the boundedness property (16) of the interpolator along with the continuous a priori estimate (11) on the velocity to write

$$\|\underline{\hat{\boldsymbol{u}}}_h\|_{1,h} \le C_I |\boldsymbol{u}|_{H^1(\Omega)^3} \le \nu^{-1} C_I C_P \|\boldsymbol{g}\|_{L^2(\Omega)^3}, \tag{75}$$

while the conclusion follows from the data-smallness assumption (68).

(i.B) *Upper bound.* To bound $\mathcal{E}_h(\underline{\boldsymbol{v}}_h)$ from above, starting from (72), we use the fact that $\boldsymbol{f} = -\nu\Delta\boldsymbol{u} + (\nabla\times\boldsymbol{u})\times\boldsymbol{u} + \nabla p$ almost everywhere in Ω, the linearity of ℓ_h in its first argument, add and subtract $\int_\Omega \nu\Delta\boldsymbol{u}\cdot\boldsymbol{v}_h$, and recall definitions (36), (43), and (49) of the consistency error linear forms to write

$$\begin{aligned} \mathcal{E}_h(\underline{\boldsymbol{v}}_h) = &\underbrace{-\int_\Omega \nu\Delta\boldsymbol{u}\cdot\boldsymbol{v}_h - \nu a_h(\underline{\boldsymbol{I}}_h^k\boldsymbol{u}, \underline{\boldsymbol{v}}_h)}_{\nu\mathcal{E}_{a,h}(\boldsymbol{u};\underline{\boldsymbol{v}}_h)} + \underbrace{\ell_h(-\nu\Delta\boldsymbol{u}, \underline{\boldsymbol{v}}_h) + \int_\Omega \nu\Delta\boldsymbol{u}\cdot\boldsymbol{v}_h}_{\mathcal{E}_{\ell,h}(-\nu\Delta\boldsymbol{u};\underline{\boldsymbol{v}}_h)} \\ &\cancel{-b_h(\underline{\boldsymbol{v}}_h, \hat{p}_h) + \ell_h(\nabla p, \underline{\boldsymbol{v}}_h)} + \underbrace{\ell_h((\nabla\times\boldsymbol{u})\times\boldsymbol{u}, \underline{\boldsymbol{v}}_h) - t_h(\underline{\hat{\boldsymbol{u}}}_h, \underline{\hat{\boldsymbol{u}}}_h, \underline{\boldsymbol{v}}_h)}_{\mathcal{E}_{t,h}(\boldsymbol{u};\underline{\boldsymbol{v}}_h)}, \end{aligned} \tag{76}$$

where we have used (41) with $\boldsymbol{g} = \boldsymbol{0}$ and ψ replaced by p in the cancellation. Thus, taking absolute values and using the consistency properties (35) of a_h, (42) of ℓ_h, and (48) of t_h, we arrive at

$$|\mathcal{E}_h(\underline{\boldsymbol{v}}_h)| \lesssim h^{k+1}\left(\nu|\boldsymbol{u}|_{H^{k+2}(\mathcal{T}_h)^3} + \|\boldsymbol{u}\|_{W^{1,4}(\Omega)^3}|\boldsymbol{u}|_{W^{k+1,4}(\mathcal{T}_h)^3}\right)\|\underline{\boldsymbol{v}}_h\|_{1,h}. \tag{77}$$

(i.C) *Estimate on the velocity.* Making $\underline{\boldsymbol{v}}_h = \underline{\boldsymbol{e}}_h$ in (77) and combining with (74) proves the estimate on the velocity error in (69).

(ii) *Estimate on the pressure.* Let us now estimate the error on the pressure. Starting from the stability property (39) of b_h and using the error equation (73), we write

$$\|\epsilon_h\|_{L^2(\Omega)} \lesssim \sup_{\underline{\boldsymbol{v}}_h \in \underline{\boldsymbol{U}}_{h,0}^k, \|\underline{\boldsymbol{v}}_h\|_{1,h}=1} \left[\mathcal{E}_h(\underline{\boldsymbol{v}}_h) - \nu a_h(\underline{\boldsymbol{e}}_h, \underline{\boldsymbol{v}}_h) - t_h(\underline{\boldsymbol{u}}_h, \underline{\boldsymbol{u}}_h, \underline{\boldsymbol{v}}_h) + t_h(\underline{\hat{\boldsymbol{u}}}_h, \underline{\hat{\boldsymbol{u}}}_h, \underline{\boldsymbol{v}}_h)\right]. \tag{78}$$

By trilinearity of t_h, it holds

$$t_h(\underline{\boldsymbol{u}}_h, \underline{\boldsymbol{u}}_h, \underline{\boldsymbol{v}}_h) - t_h(\hat{\underline{\boldsymbol{u}}}_h, \hat{\underline{\boldsymbol{u}}}_h, \underline{\boldsymbol{v}}_h) = t_h(\underline{\boldsymbol{e}}_h, \underline{\boldsymbol{u}}_h, \underline{\boldsymbol{v}}_h) + t_h(\hat{\underline{\boldsymbol{u}}}_h, \underline{\boldsymbol{e}}_h, \underline{\boldsymbol{v}}_h).$$

Plugging this equation into (78), using the bounds (77), (34), and (47), and multiplying the resulting inequality by ν^{-1}, we obtain

$$\begin{aligned}\nu^{-1}\|\epsilon_h\|_{L^2(\Omega)} \lesssim h^{k+1}\left(|\boldsymbol{u}|_{H^{k+2}(\mathcal{T}_h)^3} + \nu^{-1}\|\boldsymbol{u}\|_{W^{1,4}(\Omega)^3}|\boldsymbol{u}|_{W^{k+1,4}(\mathcal{T}_h)^3}\right)\\ + \|\underline{\boldsymbol{e}}_h\|_{1,h} + \nu^{-1}\|\underline{\boldsymbol{e}}_h\|_{1,h}\left(\|\underline{\boldsymbol{u}}_h\|_{1,h} + \|\hat{\underline{\boldsymbol{u}}}_h\|_{1,h}\right).\end{aligned}$$

We conclude using the estimate on $\|\underline{\boldsymbol{e}}_h\|_{1,h}$ already established in (69) and combining the a priori estimates (66) and (75) with the data smallness assumption (68) to write

$$\|\underline{\boldsymbol{u}}_h\|_{1,h} + \|\hat{\underline{\boldsymbol{u}}}_h\|_{1,h} \lesssim \nu^{-1}\|\boldsymbol{g}\|_{L^2(\Omega)^3} \lesssim \nu. \qquad \square$$

6 Numerical tests

In this section we propose an extensive numerical validation of the proposed method, including comparisons with the original HHO method of [7]. Our implementation is based on the `SpaFEDTe` library[1] and makes extensive use of the linear algebra `Eigen` open-source library [27]. All the steady-state computations presented hereafter are performed by means of the pseudo-transient-continuation algorithm analyzed by [29] employing the Selective Evolution Relaxation (SER) strategy [37] for evolving the pseudo-time step according to the Newton's equations residual. Convergence to steady-state is achieved when the Euclidean norm of the residual for the momentum equation drops below 10^{-12}. At each pseudo-time step, the linearised equations are exactly solved by means of the direct solver Pardiso [44], distributed as part of the Intel Math Kernel Library (Intel MKL). Accordingly, the Euclidean norm of the residual for the continuity equation is comparable to the machine epsilon at all pseudo-time steps.

6.1 Kovasznay flow

The first numerical example is meant to assess the convergence rates of the method. Let $\Omega = (-0.5, 1.5)\times(0, 2)$. We solve the Dirichlet problem corresponding to the exact solution $(\boldsymbol{u}, p)$ of [30] such that, defining the global Reynolds number $\mathrm{Re} = \frac{1}{2\nu}$ and letting $\lambda := \mathrm{Re} - \left(\mathrm{Re}^2 + 4\pi^2\right)^{\frac{1}{2}}$, the velocity components are given by

$$u_1(\boldsymbol{x}) := 1 - \exp(\lambda x_1)\cos(2\pi x_2), \qquad u_2(\boldsymbol{x}) := \frac{\lambda}{2\pi}\exp(\lambda x_1)\sin(2\pi x_2),$$

while the pressure is given by

$$p(\boldsymbol{x}) := -\frac{1}{2}\exp(2\lambda x_1) + \frac{\lambda}{2}\left(\exp(4\lambda) - 1\right).$$

We take here $\nu = 0.025$, corresponding to $\mathrm{Re} = 20$, and consider computations with polynomial degrees $k \in \{0, \ldots, 3\}$ over a sequence of uniformly h-refined simplicial grids. The Figure 1 shows the coarsest mesh used. Recall the notation of Theorem 11 and let, for the sake of brevity,

$$\underline{\boldsymbol{e}}_h := \underline{\boldsymbol{u}}_h - \hat{\underline{\boldsymbol{u}}}_h, \qquad \epsilon_h := p_h - \hat{p}_h.$$

[1] http://spafedte.github.io

We monitor the following quantities in Table 1: N_{dof} and N_{nz} denoting, respectively, the number of discrete unknowns and nonzero entries of the statically condensed linearized problem; $\|\boldsymbol{e}_h\|_{\nu,h} \coloneqq (\nu \mathrm{a}_h(\boldsymbol{e}_h, \boldsymbol{e}_h))^{\frac{1}{2}}$, the energy norm of the error on the velocity. By virtue of the global norm equivalence (34), an estimate in h^{k+1} for this quantity is readily inferred from (69); $\|\boldsymbol{e}_h\|_{L^2(\Omega)^d}$ and $\|\epsilon_h\|_{L^2(\Omega)}$, the L^2-errors on the velocity and the pressure, respectively. Each error measure is accompanied by the Estimated Order of Convergence (EOC) which, denoting by e_i an error on the ith mesh refinement characterized by the meshsize h_i, is computed as

$$\mathrm{EOC} = \frac{\log e_i - \log e_{i+1}}{\log h_i - \log h_{i+1}}.$$

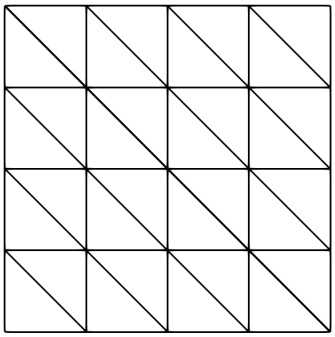

Figure 1: Coarsest mesh used in Section 6.1 .

The results collected in Table 1 show that both the energy norm of the error on the velocity and the L^2-norm of error on the pressure converge as h^{k+1} as expected. Additionally, the L^2-norm of the error of the velocity converges as h^{k+2}. This numerical observation is coherent with the theoretical results for the Stokes problem; see, in particular, [19, Theorem 7].

6.2 Robustness of the velocity error estimate

The second numerical example, inspired by [34, Benchmark 3.3], is meant to demonstrate the robustness of the proposed method for large irrotational body forces. Specifically, we want to assess numerically the fact that the approximation of the velocity is independent of both λ and p. Letting $\Omega = (0,1)^2$ and $\lambda \geq 0$, we solve the Dirichlet problem corresponding to the exact solution $(\boldsymbol{u}, p)$ in (1) with velocity components given by

$$u_1(\boldsymbol{x}) \coloneqq -y, \qquad u_2(\boldsymbol{x}) \coloneqq x,$$

and pressure given by

$$p(\boldsymbol{x}) \coloneqq \lambda x_1^3 + \frac{x_1^2 + x_2^2}{2} - \frac{1}{4}.$$

We set $\nu = 1$, then observe that the force in (1a) is purely irrotational, i.e.,

$$f_1(\boldsymbol{x}) = 3\lambda x_1^2, \qquad f_2(\boldsymbol{x}) = 0.$$

In the computations, we take $\lambda \in \{10, 10^6\}$ and consider polynomial degrees $k \in \{0, \ldots, 3\}$ over a sequence of uniformly h-refined simplicial grids. The coarsest mesh used here is similar to the one showed in the Figure 1. Tables 2 and 4 collect the numerical results for $\lambda = 10$ and $\lambda = 10^6$,

N_{dof}	$\|\underline{\boldsymbol{e}}_h\|_{\nu,h}$	EOC	$\|\boldsymbol{e}_h\|_{L^2(\Omega)^d}$	EOC	$\|\epsilon_h\|_{L^2(\Omega)}$	EOC
			$k = 0$			
80	1.39e+00	–	6.75e-01	–	1.17e+00	–
352	6.65e-01	1.06	3.20e-01	1.08	3.54e-01	1.72
1472	4.02e-01	0.73	1.17e-01	1.46	1.58e-01	1.17
6016	2.13e-01	0.91	3.37e-02	1.80	6.00e-02	1.40
24320	1.09e-01	0.97	8.85e-03	1.93	2.52e-02	1.25
			$k = 1$			
160	6.84e-01	–	3.98e-01	–	4.35e-01	–
704	1.56e-01	2.13	4.85e-02	3.04	6.26e-02	2.80
2944	4.21e-02	1.89	5.07e-03	3.26	1.19e-02	2.40
12032	1.10e-02	1.94	6.27e-04	3.01	2.84e-03	2.06
48640	2.80e-03	1.97	7.91e-05	2.99	7.04e-04	2.01
			$k = 2$			
240	1.47e-01	–	7.28e-02	–	1.16e-01	–
1056	2.22e-02	2.73	3.65e-03	4.32	7.54e-03	3.95
4416	2.95e-03	2.91	2.49e-04	3.88	8.18e-04	3.20
18048	3.74e-04	2.98	1.65e-05	3.92	9.96e-05	3.04
72960	4.70e-05	2.99	1.05e-06	3.97	1.24e-05	3.01
			$k = 3$			
320	4.42e-02	–	1.44e-02	–	1.77e-02	–
1408	2.29e-03	4.27	3.50e-04	5.36	7.60e-04	4.54
5888	1.46e-04	3.97	1.09e-05	5.01	4.85e-05	3.97
24064	9.38e-06	3.96	3.57e-07	4.93	3.04e-06	3.99
97280	5.94e-07	3.98	1.14e-08	4.97	1.90e-07	4.00

Table 1: Convergence rates for the numerical test of Section 6.1.

N_{dof}	$\|\underline{\boldsymbol{e}}_h\|_{\nu,h}$	EOC	$\|\boldsymbol{e}_h\|_{L^2(\Omega)^d}$	EOC	$\|\epsilon_h\|_{L^2(\Omega)}$	EOC
			$k = 0$			
113	2.30e-15	–	1.60e-16	–	4.94e-02	–
481	4.70e-15	-1.03	2.15e-16	-0.42	2.50e-02	0.98
1985	1.05e-14	-1.16	5.04e-16	-1.23	1.25e-02	1.00
8065	2.23e-14	-1.08	9.44e-16	-0.90	6.27e-03	1.00
32513	1.05e-13	-2.23	1.25e-14	-3.72	3.14e-03	1.00
			$k = 1$			
193	6.32e-15	–	4.86e-16	–	1.45e-02	–
833	1.39e-14	-1.14	6.10e-16	-0.33	3.64e-03	1.99
3457	3.31e-14	-1.25	1.76e-15	-1.53	9.12e-04	2.00
14081	7.26e-14	-1.14	3.09e-15	-0.82	2.28e-04	2.00
56833	1.85e-13	-1.35	1.07e-14	-1.79	5.70e-05	2.00
			$k = 2$			
273	1.14e-14	–	5.57e-16	–	5.28e-04	–
1185	2.79e-14	-1.29	1.14e-15	-1.03	6.60e-05	3.00
4929	6.76e-14	-1.28	3.01e-15	-1.41	8.25e-06	3.00
20097	1.46e-13	-1.11	7.58e-15	-1.33	1.03e-06	3.00
81153	4.06e-13	-1.48	2.99e-14	-1.98	1.29e-07	3.00
			$k = 3$			
353	2.33e-14	–	1.26e-15	–	6.36e-14	–
1537	5.46e-14	-1.23	2.54e-15	-1.01	8.78e-14	-0.46
6401	1.30e-13	-1.25	6.06e-15	-1.25	1.94e-13	-1.15
26113	2.97e-13	-1.20	1.33e-14	-1.13	5.33e-13	-1.46
105473	6.79e-13	-1.19	3.52e-14	-1.41	9.00e-13	-0.76

Table 2: Convergence results for the numerical test of Section 6.2, $\lambda = 10$, present formulation (65).

N_{dof}	$\|\underline{\boldsymbol{e}}_h\|_{v,h}$	EOC	$\|\boldsymbol{e}_h\|_{L^2(\Omega)^d}$	EOC	$\|\epsilon_h\|_{L^2(\Omega)}$	EOC
			$k = 0$			
113	1.61e+00	–	1.94e-01	–	3.65e-01	–
481	8.38e-01	0.94	5.28e-02	1.88	1.74e-01	1.07
1985	4.26e-01	0.98	1.37e-02	1.95	6.66e-02	1.38
8065	2.14e-01	0.99	3.48e-03	1.98	2.25e-02	1.57
32513	1.07e-01	1.00	8.75e-04	1.99	7.02e-03	1.68
			$k = 1$			
193	1.69e-01	–	1.25e-02	–	3.69e-02	–
833	4.31e-02	1.97	1.61e-03	2.96	8.58e-03	2.11
3457	1.09e-02	1.99	2.04e-04	2.98	2.12e-03	2.01
14081	2.73e-03	1.99	2.58e-05	2.99	5.34e-04	1.99
56833	6.85e-04	2.00	3.23e-06	2.99	1.34e-04	1.99
			$k = 2$			
273	7.10e-03	–	4.25e-04	–	1.89e-03	–
1185	8.98e-04	2.98	2.70e-05	3.98	2.39e-04	2.99
4929	1.13e-04	2.99	1.70e-06	3.99	3.00e-05	2.99
20097	1.42e-05	3.00	1.07e-07	3.99	3.76e-06	3.00
81153	1.77e-06	3.00	6.69e-09	4.00	4.70e-07	3.00
			$k = 3$			
353	2.46e-14	–	1.61e-15	–	3.69e-14	–
1537	6.00e-14	-1.29	3.81e-15	-1.24	1.01e-13	-1.45
6401	1.41e-13	-1.23	7.21e-15	-0.92	1.78e-13	-0.82
26113	3.29e-13	-1.22	1.67e-14	-1.21	5.41e-13	-1.60
105473	7.27e-13	-1.14	4.75e-14	-1.51	1.01e-12	-0.90

Table 3: Convergence results for the numerical test of Section 6.2, $\lambda = 10$, original HHO formulation of [7].

N_{dof}	$\|\underline{\boldsymbol{e}}_h\|_{v,h}$	EOC	$\|\boldsymbol{e}_h\|_{L^2(\Omega)^d}$	EOC	$\|\epsilon_h\|_{L^2(\Omega)}$	EOC
			$k = 0$			
113	2.66e-11	–	2.15e-12	–	3.93e+03	–
481	3.62e-11	-0.44	2.28e-12	-0.08	2.00e+03	0.98
1985	3.34e-11	0.12	1.58e-12	0.52	1.00e+03	0.99
8065	4.69e-11	-0.49	1.24e-12	0.35	5.02e+02	1.00
32513	4.50e-11	0.06	1.03e-12	0.27	2.51e+02	1.00
			$k = 1$			
193	2.52e-11	–	2.69e-12	–	1.35e+03	–
833	3.92e-11	-0.64	2.32e-12	0.21	3.41e+02	1.99
3457	4.38e-11	-0.16	3.62e-12	-0.64	8.53e+01	2.00
14081	7.99e-11	-0.87	7.83e-12	-1.11	2.13e+01	2.00
56833	1.52e-10	-0.93	1.74e-11	-1.15	5.33e+00	2.00
			$k = 2$			
273	4.76e-11	–	2.80e-12	–	5.28e+01	–
1185	4.82e-11	-0.02	3.44e-12	-0.30	6.60e+00	3.00
4929	8.69e-11	-0.85	7.34e-12	-1.10	8.25e-01	3.00
20097	1.60e-10	-0.88	9.00e-12	-0.29	1.03e-01	3.00
81153	2.77e-10	-0.79	2.10e-11	-1.22	1.29e-02	3.00
			$k = 3$			
353	2.14e-11	–	9.25e-13	–	1.62e-10	–
1537	3.61e-11	-0.75	2.09e-12	-1.18	1.48e-10	0.13
6401	5.94e-11	-0.72	3.94e-12	-0.92	1.89e-10	-0.35
26113	6.17e-11	-0.06	2.10e-12	0.91	1.46e-10	0.38
105473	1.01e-10	-0.71	9.28e-12	-2.14	3.91e-10	-1.43

Table 4: Convergence results for the numerical test of Section 6.2, $\lambda = 10^6$, present formulation (65).

N_{dof}	$\|\|\underline{\boldsymbol{e}}_h\|\|_{\nu,h}$	EOC	$\|\|\boldsymbol{e}_h\|\|_{L^2(\Omega)^d}$	EOC	$\|\|\epsilon_h\|\|_{L^2(\Omega)}$	EOC
			$k = 0$			
113	1.53e+05	–	1.80e+04	–	4.55e+04	–
481	2.57e+06	-4.08	1.17e+05	-2.70	1.21e+06	-4.73
1985	2.62e+05	3.30	6.29e+03	4.22	1.05e+05	3.53
8065	2.05e+04	3.67	3.25e+02	4.27	4.53e+03	4.53
32513	1.05e+04	0.97	8.48e+01	1.94	8.67e+02	2.39
			$k = 1$			
193	Not converged					
833	Not converged					
3457	1.05e+03	–	2.01e+01	–	2.27e+02	–
14081	2.67e+02	1.98	2.52e+00	2.99	5.34e+01	2.09
56833	6.69e+01	2.00	3.16e-01	3.00	1.34e+01	2.00
			$k = 2$			
273	4.73e+02	–	2.71e+01	–	3.19e+02	–
1185	8.98e+01	2.40	2.70e+00	3.33	2.39e+01	3.74
4929	1.13e+01	2.99	1.70e-01	3.99	3.00e+00	3.00
20097	1.42e+00	3.00	1.07e-02	3.99	3.76e-01	3.00
81153	1.77e-01	3.00	6.69e-04	4.00	4.70e-02	3.00
			$k = 3$			
353	2.62e-11	–	1.65e-12	–	1.63e-10	–
1537	4.67e-11	-0.84	4.45e-12	-1.43	1.72e-10	-0.08
6401	6.57e-11	-0.49	5.10e-12	-0.20	1.54e-10	0.16
26113	7.23e-11	-0.14	3.48e-12	0.55	1.65e-10	-0.10
105473	1.21e-10	-0.74	1.01e-11	-1.54	2.41e-10	-0.54

Table 5: Convergence results for the numerical test of Section 6.2, $\lambda = 10^6$, original HHO formulation of [7].

respectively, obtained using the formulation (65). For the sake of comparison, we also report in Tables 3 and 5 the corresponding results obtained using the original HHO method of [7].

A first important difference highlighted by the numerical results is that the velocity field is exactly reproduced by the formulation (65) proposed in this work, whereas this is not the case for the original HHO method of [7]; compare the third and fifth columns of Tables 2–5. This is a consequence of the pressure-independence of the error estimate (69) together with the fact that the we are considering an affine velocity field. A second, related, remark is that the velocity approximation for the present method is independent of λ (for both of the values considered we have zero-machine error), whereas increasing the value of λ has a strong impact on the velocity approximation for the classical HHO method of [7]; compare the third and fifth columns of Tables 3 and 5.

6.3 Two-dimensional lid-driven cavity flow

The third numerical test is the two-dimensional lid-driven cavity problem. The computational domain is the unit square $\Omega = (0,1)^2$ and we set $\boldsymbol{f} = \boldsymbol{0}$. Homogeneous (wall) boundary conditions are enforced at all but the top horizontal wall (at $x_2 = 1$), where we enforce a unit tangential velocity $\boldsymbol{u} = (1,0)$. In passing, notice that, in this classical test, the boundary condition is incompatible with the formulation (1) since the solution does not belong to $H^1(\Omega)^d$.

In Figures 2, and 3, we report the horizontal component u_1 of the velocity along the vertical centerline $x_1 = \frac{1}{2}$ and the vertical component u_2 of the velocity along the horizontal centerline $x_2 = \frac{1}{2}$ for the two dimensional flow at global Reynolds numbers $\mathrm{Re} := \frac{1}{\nu}$ respectively equal to 1,000, and 5,000. The reference computation is carried out setting $k = 1$ and using a uniform structured simplicial mesh obtained starting from a 64×64 decomposition of the domain. For instance, the Figure 1 shows the 4×4 decomposition of the current domain. For the sake of comparison, we also include very high-order computations with $k = 5$ on structured simplicial meshes obtained starting from 16×16 and 32×32 decompositions of the domain for $\mathrm{Re} = 1{,}000$ and $\mathrm{Re} = 5{,}000$, respectively. References solutions from the literature [23, 25] are also included for the sake of comparison. The numerical solution obtained using the proposed method is in excellent agreement with the reference results for both values of the Reynolds number. For $\mathrm{Re} = 5{,}000$, the very high-order computation gives sharper transitions close to the walls which, as noticed in [7], seem more physically sound.

To check the robustness of the method with respect to irrotational body forces, we then run the same test case but with

$$\boldsymbol{f} = \lambda \nabla \psi,$$

where $\psi = \frac{1}{3}(x^3 + y^3)$. Observe that this body force is completely irrotational, so the velocity approximation obtained using the proposed method (65) should not be affected (and, therefore, should not depend on λ). To verify this, we report in Figure 4 computations for $\mathrm{Re} = 1{,}000$ and $\lambda \in \{10^3, 10^6\}$, using $k = 1$, and the simplicial mesh obtained starting from a 64×64 decomposition of the domain. As expected, the velocity profiles are not affected by the value of λ. The same plot also contains the results obtained with the original HHO formulation of [7], but only for $\lambda = 10^3$ (convergence was not achieved for $\lambda = 10^6$). In this case, the velocity profiles are clearly affected by the presence of the body force, and large oscillations are observed with this value of λ.

Conlcusion

We have extended the HHO method of [19] to the fully nonlinear Navier–Stokes problem by introducing a novel HHO discretisation of the convective trilinear form based on a velocity reconstruction in the local Raviart–Thomas–Nédélec space obtained working element by element. On matching simplicial meshes, this extension results in a method robust for large irrotational body forces which

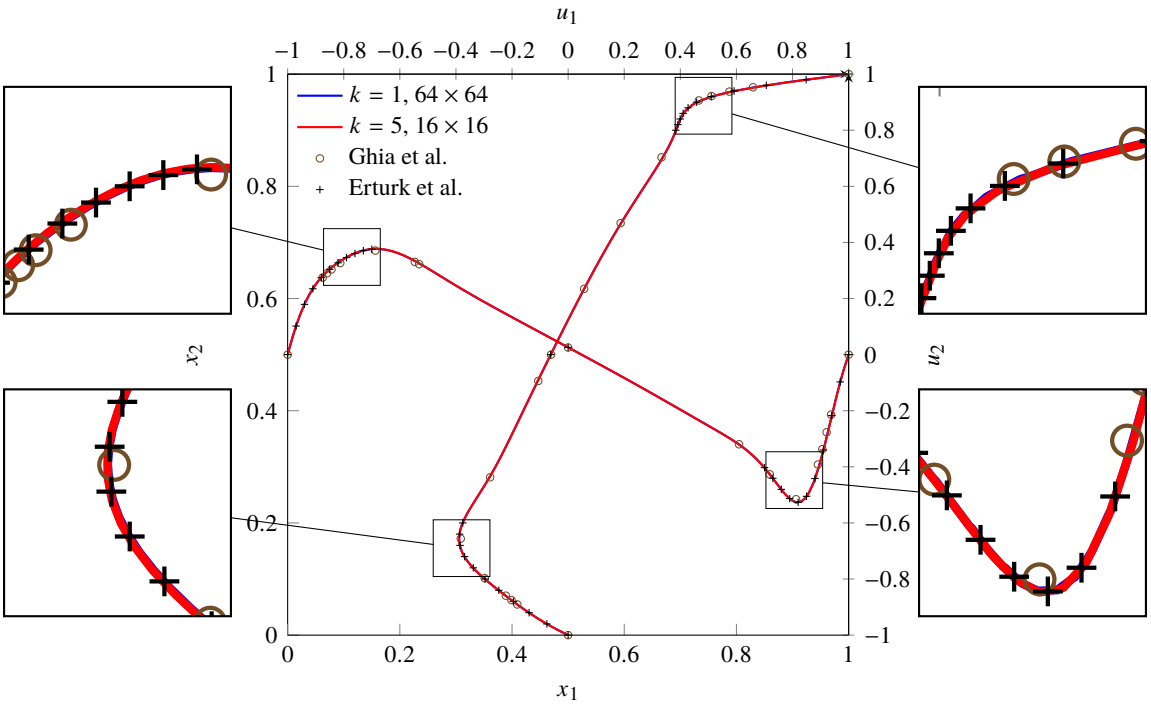

Figure 2: Two-dimensional lid-driven cavity flow, horizontal component u_1 of the velocity along the vertical centerline $x_1 = \frac{1}{2}$ and the vertical component u_2 of the velocity along the horizontal centerline $x_2 = \frac{1}{2}$ for Re = 1,000.

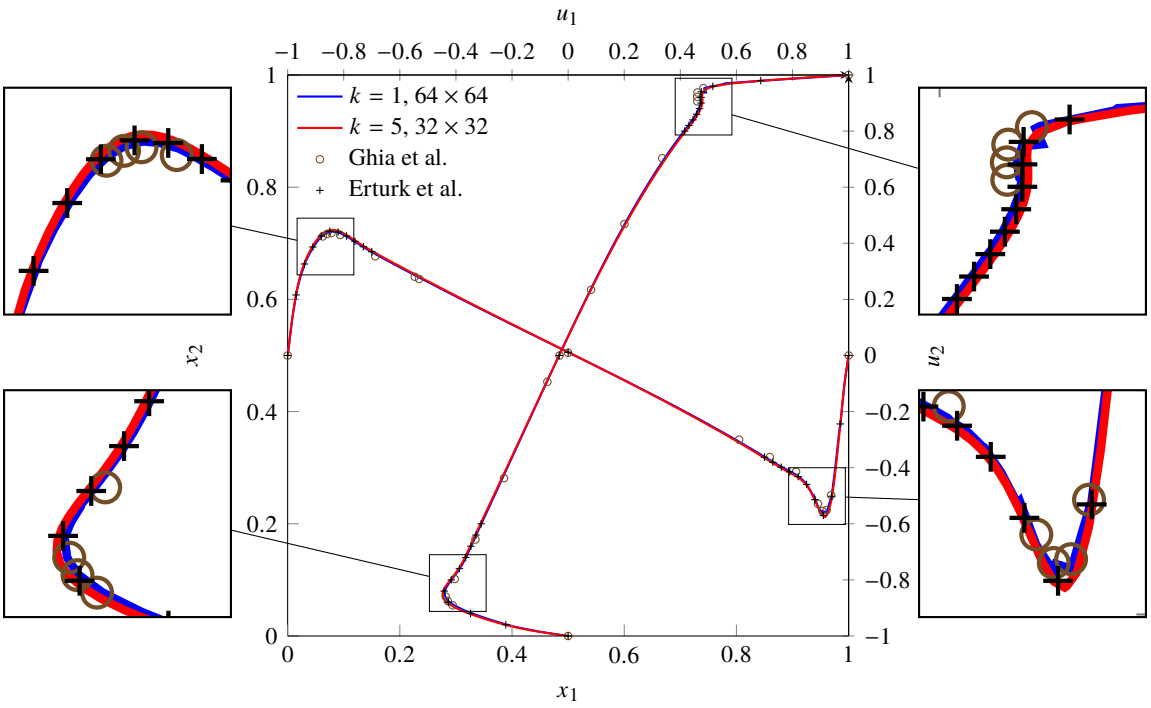

Figure 3: Two-dimensional lid-driven cavity flow, horizontal component u_1 of the velocity along the vertical centerline $x_1 = \frac{1}{2}$ and the vertical component u_2 of the velocity along the horizontal centerline $x_2 = \frac{1}{2}$ for Re = 5,000

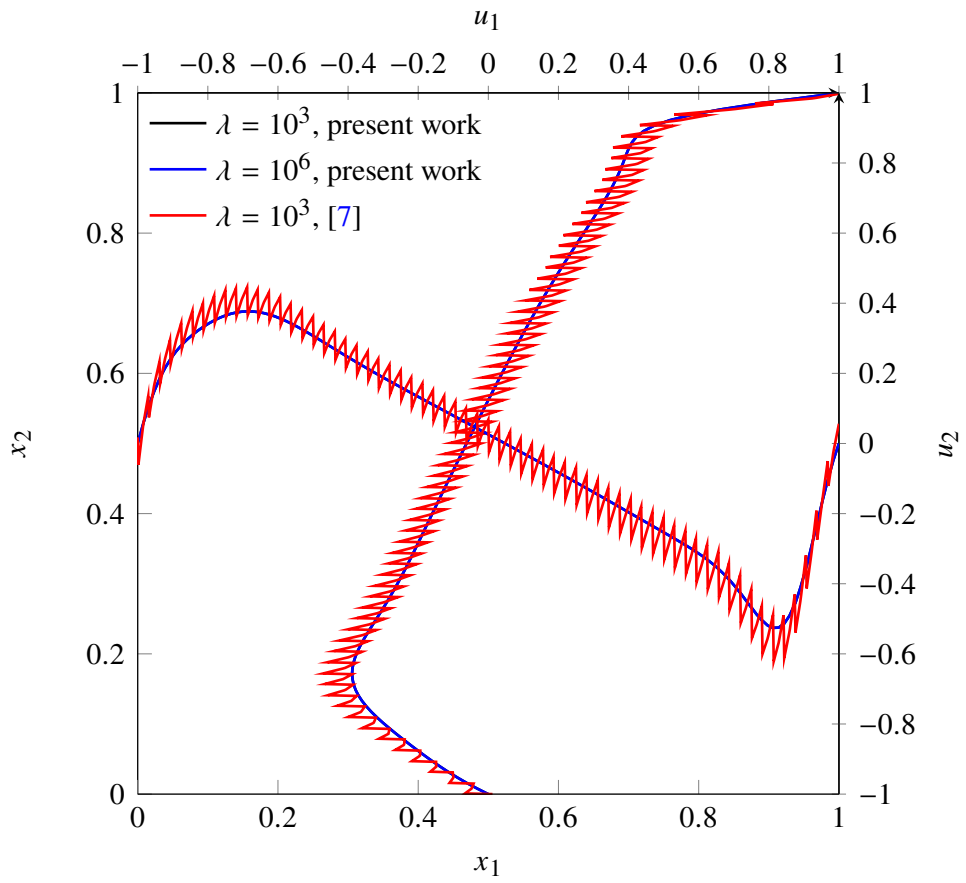

Figure 4: Two-dimensional lid-driven cavity flow with irrotational force $\boldsymbol{f} = \lambda \nabla \psi$ with $\lambda \in \{10^3, 10^6\}$. Comparison between the present method and the original HHO formulation of [7]. The plot represents the horizontal component u_1 of the velocity along the vertical centerline $x_1 = \frac{1}{2}$ and the vertical component u_2 of the velocity along the horizontal centerline $x_2 = \frac{1}{2}$ for Re = 1,000.

preserves the order of convergence of the original one. We have presented two-dimensional numerical studies illustrating the performance of the proposed method, as well as the benefits compared to more standard formulations. Three-dimensional numerical tests are left for a future, application-oriented publication. The extension of the divergence-free velocity reconstruction of Section 3.4 to general polygonal and polyhedral meshes is currently under development.

Acknowledgements

This work was partially supported by *Agence Nationale de la Recherche* grant HHOMM (ANR-15-CE40-0005). The first author also acknowledges the support of *Agence pour les mathématiques en interaction avec l'entreprise et la société*. The second author also acknowledges the support of *Agence Nationale de la Recherche* grant fast4hho (ANR-17-CE23-0019).

References

[1] N. Ahmed, A. Linke, and C. Merdon. "Towards pressure-robust mixed methods for the incompressible Navier-Stokes equations". In: *Comput. Methods Appl. Math.* 18.3 (2018), pp. 353–372. DOI: 10.1515/cmam-2017-0047.

[2] D. Arnold. *Finite Element Exterior Calculus*. SIAM, 2018. ISBN: 978-1-611975-53-6.

[3] L. Beirão da Veiga, F. Dassi, and G. Vacca. "The Stokes complex for Virtual Elements in three dimensions". In: *arXiv e-prints*, arXiv:1905.01579 (2019), arXiv:1905.01579. arXiv: 1905.01579 [math.NA].

[4] L. Beirão da Veiga, C. Lovadina, and G. Vacca. "Divergence free Virtual Elements for the Stokes problem on polygonal meshes". In: *ESAIM: Math. Model. Numer. Anal. (M2AN)* 51.2 (2017), pp. 509–535. DOI: 10.1051/m2an/2016032.

[5] L. Beirão da Veiga, C. Lovadina, and G. Vacca. "Virtual Elements for the Navier–Stokes Problem on Polygonal Meshes". In: *SIAM J. Numer. Anal.* 56.3 (2018), pp. 1210–1242. DOI: 10.1137/17M1132811.

[6] D. Boffi, F. Brezzi, and M. Fortin. *Mixed finite element methods and applications*. Vol. 44. Springer Series in Computational Mathematics. Heidelberg: Springer, 2013, pp. xiv+685. DOI: 10.1007/978-3-642-36519-5.

[7] L. Botti, D. A. Di Pietro, and J. Droniou. "A Hybrid High-Order method for the incompressible Navier-Stokes equations based on Temam's device". In: *Journal of Computational Physics* 376 (2019), pp. 786–816. DOI: 10.1016/j.jcp.2018.10.014.

[8] S. C. Brenner and R. Scott. *The mathematical theory of finite element methods*. Third. Vol. 15. Texts in Applied Mathematics. New York: Springer, 2008, pp. xviii+397. ISBN: 978-0-387-75933-3. DOI: 10.1007/978-0-387-75934-0.

[9] J. Carrero, B. Cockburn, and D. Schötzau. "Hybridized globally divergence-free LDG methods. Part I: The Stokes problem". In: *Math. Comput.* 75 (2005), pp. 533–563.

[10] A. Çeşmelioğlu, B. Cockburn, and W. Qiu. "Analysis of a hybridizable discontinuous Galerkin method for the steady-state incompressible Navier-Stokes equations". In: *Math. Comput.* 86 (2017), pp. 1643–1670.

[11] A. Çeşmelioğlu, B. Cockburn, N. C. Nguyen, and J. Peraire. "Analysis of HDG methods for Oseen equations". In: *J. Sci. Comput.* 55.2 (2013), pp. 392–431. DOI: 10.1007/s10915-012-9639-y.

[12] L. Chen and F. Wang. "A Divergence Free Weak Virtual Element Method for the Stokes Problem on Polytopal Meshes". In: *Journal of Scientific Computing* 78.2 (2019), pp. 864–886. DOI: 10.1007/s10915-018-0796-5.

[13] P. Ciarlet. *The Finite Element Method for Elliptic Problems*. Society for Industrial and Applied Mathematics, 2002. DOI: 10.1137/1.9780898719208. URL: https://epubs.siam.org/doi/abs/10.1137/1.9780898719208.

[14] B. Cockburn, D. A. Di Pietro, and A. Ern. "Bridging the Hybrid High-Order and Hybridizable Discontinuous Galerkin methods". In: *ESAIM: Math. Model Numer. Anal.* 50.3 (2016), pp. 635–650. DOI: 10.1051/m2an/2015051.

[15] B. Cockburn, N. C. Nguyen, and J. Peraire. "A comparison of HDG methods for Stokes flow". In: *J. Sci. Comput.* 45.1-3 (2010), pp. 215–237. DOI: 10.1007/s10915-010-9359-0.

[16] M. Crouzeix and P.-A. Raviart. "Conforming and nonconforming finite element methods for solving the stationary Stokes equations". In: *RAIRO Modél. Math. Anal. Num.* 7.3 (1973), pp. 33–75.

[17] D. A. Di Pietro and J. Droniou. *The Hybrid High-Order Method for Polytopal Meshes - Design, Analysis and Applications*. Submitted. 2019.

[18] D. A. Di Pietro and R. Tittarelli. "Numerical Methods for PDEs. State of the Art Techniques". In: ed. by L. F. D. A. Di Pietro A. Ern. SEMA-SIMAI 15. Springer, 2018. Chap. An introduction to Hybrid High-Order methods. ISBN: 978-3-319-94675-7 (Print) 978-3-319-94676-4 (eBook). DOI: 10.1007/978-3-319-94676-4_4.

[19] D. A. Di Pietro, A. Ern, A. Linke, and F. Schieweck. "A discontinuous skeletal method for the viscosity-dependent Stokes problem". In: *Computer Methods in Applied Mechanics and Engineering* 306 (2016), pp. 175–195. DOI: 10.1016/j.cma.2016.03.033.

[20] D. A. Di Pietro and J. Droniou. "A Hybrid High-Order method for Leray-Lions elliptic equations on general meshes". In: *Math. Comp.* 86 (2017), pp. 2159–2191. DOI: 10.1090/mcom/3180.

[21] D. A. Di Pietro and S. Krell. "A Hybrid High-Order Method for the Steady Incompressible Navier–Stokes Problem". In: *Journal of Scientific Computing* 74.3 (2018), pp. 1677–1705. DOI: 10.1007/s10915-017-0512-x.

[22] T. Dupont and R. Scott. "Polynomial approximation of functions in Sobolev spaces". In: *Math. Comput.* 34.150 (1980), pp. 441–463. DOI: 10.2307/2006095.

[23] E. Erturk, T. C. Corke, and C. Gökçöl. "Numerical solutions of 2-D steady incompressible driven cavity flow at high Reynolds". In: *Int. J. Numer. Meth. Fluids* 48.7 (2005), pp. 747–774. DOI: 10.1002/fld.953.

[24] G. N. Gatica. *A Simple Introduction to the Mixed Finite Element Method: Theory and Applications*. SpringerBriefs in Mathematics. Cham: Springer, 2014. URL: http://cds.cern.ch/record/1646889.

[25] U. Ghia, K. Ghia, and C. Shin. "High-Re solutions for incompressible flow using the Navier–Stokes equations and a multigrid method". In: *J. Comput. Phys.* 48.3 (1982), pp. 387–411. DOI: 10.1016/0021-9991(82)90058-4.

[26] G. Giorgiani, S. Fernández-Méndez, and A. Huerta. "Hybridizable Discontinuous Galerkin with degree adaptivity for the incompressible Navier–Stokes equations". In: *Computers & Fluids* 98 (2014), pp. 196–208. DOI: 10.1016/j.compfluid.2014.01.011.

[27] B. Guennebaud G. and Jacob and et al. “Eigen v3”. In: (2010). URL: http://eigen.tuxfamily.org.

[28] V. John. *Finite Element Methods for Incompressible Flow Problems*. Springer International Publishing, Switzerland, 2016.

[29] C. Kelley and D. Keyes. “Convergence analysis of pseudo-transient continuation”. In: *SIAM Journal on Numerical Analysis* 35.2 (1998), pp. 508–523. DOI: 10.1137/S0036142996304796. URL: http://dx.doi.org/10.1137/S0036142996304796.

[30] L. I. G. Kovasznay. “Laminar flow behind a two-dimensional grid”. In: *Proceedings of the Cambridge Philosophical Society* 44.1 (1948), pp. 58–62. DOI: 10.1017/S0305004100023999. URL: http://dx.doi.org/10.1017/S0305004100023999.

[31] R. J. Labeur and G. N. Wells. “A Galerkin interface stabilisation method for the advection-diffusion and incompressible Navier-Stokes equations”. In: *Comput. Methods Appl. Mech. Engrg.* 196.49-52 (2007), pp. 4985–5000. DOI: 10.1016/j.cma.2007.06.025.

[32] C. Lehrenfeld. “Hybrid Discontinuous Galerkin methods for solving incompressible flow problems”. PhD thesis. Rheinisch-Westfälischen Technischen Hochschule Aachen, 2010.

[33] C. Lehrenfeld and J. Schöberl. “High order exactly divergence-free Hybrid Discontinuous Galerkin Methods for unsteady incompressible flows”. In: *Computer Methods in Applied Mechanics and Engineering* 307 (2016), pp. 339 –361. DOI: 10.1016/j.cma.2016.04.025.

[34] A. Linke and C. Merdon. “On velocity errors due to irrotational forces in the Navier-Stokes momentum balance”. In: *Journal of Computational Physics* 313 (2016), pp. 654–661. DOI: 10.1016/j.jcp.2016.02.070.

[35] A. Linke and C. Merdon. “Pressure-robustness and discrete Helmholtz projectors in mixed finite element methods for the incompressible Navier-Stokes equations”. In: *Comput. Methods Appl. Mech. Engrg.* 311 (2016), pp. 304–326. DOI: 10.1016/j.cma.2016.08.018.

[36] A. Linke. “On the role of the Helmholtz decomposition in mixed methods for incompressible flows and a new variational crime”. In: *Comput. Methods Appl. Mech. Engrg.* 268 (2014), pp. 782–800. DOI: 10.1016/j.cma.2013.10.011.

[37] W. A. Mulder and B. Van Leer. “Experiments with implicit upwind methods for the Euler equations”. In: *J. Comput. Phys.* 59.2 (1985), pp. 232 –246. DOI: 10.1016/0021-9991(85)90144-5.

[38] J. C. Nédélec. “Mixed Finite Elements in $\mathbb{R}^3$”. In: *Numer. Math.* 35 (1980), pp. 315–341. DOI: 10.1007/BF01396415.

[39] I. Oikawa. “A hybridized discontinuous Galerkin method with reduced stabilization”. In: *J. Sci. Comput.* 65.1 (2015), pp. 327–340. DOI: 10.1007/s10915-014-9962-6.

[40] W. Qiu and K. Shi. “A superconvergent HDG method for the incompressible Navier–Stokes equations on general polyhedral meshes”. In: *IMA J. Numer. Anal.* 36.4 (2016), pp. 1943–1967. DOI: 10.1093/imanum/drv067.

[41] P. A. Raviart and J. M. Thomas. “A mixed finite element method for 2nd order elliptic problems”. In: *Mathematical Aspects of the Finite Element Method, Lecture Notes in Mathematics* 606 (1977), pp. 292–315.

[42] S. Rhebergen and B. Cockburn. “A space-time hybridizable discontinuous Galerkin method for incompressible flows on deforming domains”. In: *J. Comput. Phys.* 231.11 (2012), pp. 4185–4204. DOI: 10.1016/j.jcp.2012.02.011.

[43] S. Rhebergen and G. N. Wells. “A Hybridizable Discontinuous Galerkin Method for the Navier–Stokes Equations with Pointwise Divergence-Free Velocity Field”. In: *Journal of Scientific Computing* 76.3 (2018), pp. 1484–1501. DOI: 10.1007/s10915-018-0671-4.

[44] O. Schenk, K. Gärtner, W. Fichtner, and A. Stricker. “Pardiso: A high-performance serial and parallel sparse linear solver in semiconductor device simulation”. In: *Future Gener. Comput. Syst.* 18.1 (2001), pp. 69–78. DOI: 10.1016/S0167-739X(00)00076-5.

[45] M. P. Ueckermann and P. F. J. Lermusiaux. “Hybridizable discontinuous Galerkin projection methods for Navier-Stokes and Boussinesq equations”. In: *J. Comput. Phys.* 306 (2016), pp. 390–421. DOI: 10.1016/j.jcp.2015.11.028.